

Globally Optimal Movable Antenna-Enhanced multi-user Communication: Discrete Antenna Positioning, Motion Power Consumption, and Imperfect CSI

Yifei Wu*, Dongfang Xu[†], Derrick Wing Kwan Ng[‡], Wolfgang Gerstacker*, and Robert Schober*

*Friedrich-Alexander-Universität Erlangen-Nürnberg, Germany [‡]The University of New South Wales, Australia

[†]The Hong Kong University of Science and Technology, Hong Kong

Abstract

Movable antennas (MAs) represent a promising paradigm to enhance the spatial degrees of freedom of conventional multi-antenna systems by dynamically adapting the positions of antenna elements within a designated transmit area. In particular, by employing electro-mechanical MA drivers such as stepper motors, the positions of the MA elements can be discretely adjusted to shape a favorable spatial correlation for improving system performance. Although preliminary research has explored beamforming designs for MA-enabled systems, the intricacies of the power consumption and the precise positioning of MA elements are not well understood. Moreover, the assumption of perfect channel state information (CSI) adopted in the current literature is generally impractical due to the significant pilot overhead and the extensive time required for acquiring perfect CSI. To address these challenges, in this paper, we model the motion of MA elements through discrete steps and quantify the associated power consumption as a function of these movements. Furthermore, by leveraging the properties of the MA channel model, we introduce a novel CSI error model tailored for MA-enabled systems that facilitates robust resource allocation design. In particular, we jointly optimize the beamforming and the MA positions at the base station (BS) for minimization of the total BS power consumption, encompassing both radiated power and MA motion power, while guaranteeing a minimum required signal-to-interference-plus-noise ratio (SINR) for each user. To this end, novel algorithms exploiting the branch and bound (BnB) method are developed to obtain the globally optimal solution for perfect and imperfect CSI, respectively. Moreover, to support practical real-time implementation, we propose low-complexity suboptimal algorithms with guaranteed convergence by leveraging successive convex approximation (SCA). Our numerical results validate the global optimality of the proposed BnB-based algorithms for both CSI scenarios. Furthermore, we unveil that both proposed SCA-based algorithms approach the optimal performance of the BnB-based algorithms within only

This work has been presented in part at the IEEE Global Communications Conference, Kuala Lumpur, Malaysia, December 2023 [1].

a few iterations, thus highlighting their practical advantages. Additionally, we show that compared to the state-of-the-art alternating-optimization-based approach, the proposed low-complexity SCA-based schemes achieve considerable performance gains, especially in high-load systems with a small number of antenna elements.

I. INTRODUCTION

Multiple-input multiple-output (MIMO) transmission has been widely recognized as a key technique to satisfy the skyrocketing data traffic demands of sixth-generation (6G) networks. Through the deployment of multiple antennas, MIMO can effectively utilize the spatial resources of wireless channels to deliver significant enhancements in performance, including higher data transmission rates [2], improved physical layer security [3], and the realization of innovative paradigms such as integrated sensing and communication (ISAC) [4]. However, despite these benefits, conventional MIMO systems suffer from elevated hardware costs and computational complexity due to the requirement of equipping multiple parallel power-hungry radio frequency (RF) chains [2]. To address this challenge, antenna selection (AS) has been advocated as a realistic strategy for implementing practical MIMO systems. The crux of AS is to strategically choose a small subset of antennas with favorable channel characteristics from a larger pool of candidate antennas. By delicately choosing favorable antennas, AS maintains the diversity gain of MIMO systems while reducing the number of required RF chains. Nevertheless, traditional MIMO systems, even those employing AS, encounter limitations due to the fixed positions of their antennas. In fact, this fixed arrangement restricts their ability to fully exploit spatial variations in the channel across the transmit area, potentially undermining overall system performance.

To fully capitalize on the spatial variations of wireless channels across a designated spatial transmit area, holographic MIMO has emerged as a recent groundbreaking development [5]. Specifically, holographic MIMO surfaces are composed of numerous miniature passive elements that are spaced at sub-wavelength intervals. These elements can be electronically controlled to manipulate the electromagnetic properties of transmitted or reflected waves, offering a novel approach for channel optimization and signal enhancement [6]. Therefore, the utilization of zero-spacing continuous antenna elements in holographic MIMO allows for the exploitation of the full spatial degrees of freedom (DoFs) within a spatially continuous transmit area. Indeed, this unique configuration enables a more intricate control and manipulation of the electromagnetic field, enhancing the overall performance of the communication system. However, despite the high potential of holographic MIMO to revolutionize communications systems, significant challenges arise in its implementation due to the large required number of antenna elements. This formidable challenge is further manifested in both channel estimation and data processing, limiting the practical viability of holographic MIMO [5].

Motivated by the large number of spatial DoFs potentially offered by holographic MIMO surfaces, the novel MIMO concept of movable antennas (MAs) has emerged as a promising technology, bridging the gap between holographic MIMO and traditional MIMO [7]. In MA-enabled systems, each antenna element is connected to an RF chain through a flexible cable, allowing its physical position to be dynamically adapted within a specified spatial region by an electro-mechanical driver [8] or using liquid metals [9]. Therefore, this unique capability endows MA-enabled systems with the flexibility to adjust antenna positions in real-time to establish favorable spatial antenna correlations thereby improving the performance of MIMO systems [8], [10], [11]. Moreover, since MA systems necessitate only a small number of antenna elements and RF chains to exploit the available DoFs, the computational complexity required for signal processing is significantly reduced compared to holographic MIMO systems [7], [8], [10].

Based on their hardware architecture, state-of-the-art MA systems can be categorized into two types: mechanical MA systems [1], [8], [10] and fluid antenna systems (FAS) [9], [12]. In particular, mechanical MA systems employ electro-mechanical devices such as stepper motors to move the antennas. In contrast, FAS feature antennas that can switch positions almost instantaneously in a small linear space, facilitated by the use of liquid metals. As a matter of fact, various initial works demonstrated considerable potential for both types of MA systems by jointly optimizing MA positions and base station (BS) beamforming. For instance, the concept of fluid antenna multiple access (FAMA) was introduced in [12] using a single fluid antenna for each mobile user. In FAMA, the positions of the fluid antennas at different users are strategically selected to achieve favorable channel conditions with reduced interference, thereby resulting in massive capacity gains. However, due to the inherent physical properties of liquid materials, FAS can only support a single fluid antenna in motion along a one-dimensional (1D) line. Therefore, FAS cannot fully exploit variations in the wireless channel across the two-dimensional (2D) or three-dimensional (3D) spatial domains, thereby restricting their effectiveness in complex environmental conditions. To tackle this limitation, several works have considered electro-mechanical systems as MA drivers to enable flexible movement in 2D or 3D transmit regions [1], [8]. For instance, in [8], the authors investigated scenarios in which both the BS and multiple users were equipped with MAs. To jointly optimize the MA positions and beamforming, an alternating optimization (AO)-based suboptimal algorithm was introduced. Similarly, for the multi-user mechanical MA-enabled uplink communication system in [10], the authors proposed suboptimal joint designs based on zero-forcing (ZF) and minimum mean square error (MMSE) combining, respectively. In particular, the BS employed ZF or MMSE combining, while the MA positions were adjusted with a gradient descent (GD) method. However, both [8] and [10] relied on the optimistic assumption that the electro-mechanical MA driver can position the MAs freely within a given region. In contrast, prototype

designs of MA-enabled systems, reported in, e.g., [13] and [14], reveal that the motion control of the employed electro-mechanical devices is limited to discrete adjustments with finite precision. As a result, the transmit area is spatially quantized [14], providing a finite spatial resolution rather than the infinite resolution previously assumed in [7], [8], [10]. Moreover, the existing research in [7], [8], [10] does not account for the power consumption introduced by the electro-mechanical MA driver. In fact, to facilitate rapid position adjustments of MA elements, practical MA-enabled systems necessitate the application of high-speed electro-mechanical devices as MA drivers, leading to significant power consumption. This motion power consumption highly depends on the MA position displacement, and needs to be considered for resource allocation design. In addition, existing MA-enabled system designs are based on suboptimal frameworks, e.g., the AO-based algorithm in [8] and the GD-based method in [10]. These suboptimal approaches generally compromise global optimality, and their performance heavily depends the chosen initial point, which may lead to unsatisfactory system performance. This highlights the need for optimization methods that can ensure global optimality and convergence.

Recently, in the conference version [1] of this paper, a novel algorithm based on the generalized Benders decomposition (GBD) framework was developed for attaining the globally jointly optimum BS beamformer and MA positions that minimize the radiated power of multi-user MA-enabled systems. However, the promised performance in [1] relies on the acquisition of the perfect CSI for all MA candidate positions. In fact, since the transmit area of MA-enabled systems is quantized to numerous discrete positions, it is challenging to accurately estimate the channels between all MA candidate positions and all users by conventional channel estimation methods [15], [16]. As such, channel estimation errors are generally inevitable, leading to imperfect CSI. The authors in [17], [18] have investigated statistical beamforming for MA-enabled systems assuming ideal continuous MA motion. However, for practical MA systems with imperfect CSI and discrete MA movement, neither globally optimal nor efficient suboptimal robust resource allocation frameworks are available in the literature. Motivated by the above discussion, in this paper, we investigate for the first time the globally optimal joint design of BS beamforming and MA positioning for multi-user MA-enabled systems with discrete MA movement for both perfect and imperfect CSI. The main contributions of this paper can be summarized as follows:

- In this work, we consider an MA-enabled multi-user MISO downlink communication system, where the movement of the antennas is enabled by electro-mechanical devices. In particular, for the first time, we model MA movement as a discrete motion and propose a corresponding power consumption model. Next, we study the resource allocation problem for the considered MA-enabled communication system. Specifically, the objective of the proposed resource allocation design is the minimization of the total

power consumption at the BS, which accounts for the aggregated power comprising the radiated power and the power required for MA motion, while guaranteeing a minimum signal-to-interference-plus-noise ratio (SINR) for each user.

- We first investigate the resource allocation design for the ideal case of perfect CSI. The joint BS beamforming and MA position design is formulated as a mixed integer nonlinear programming (MINLP) problem. To tackle this challenging problem, we propose a series of mathematical transformations aimed at facilitating the design of an iterative algorithm based on the branch and bound (BnB) method, which is guaranteed to converge to the globally optimal solution. This yields a performance upper bound for resource allocation design in MA systems with perfect CSI and serves as a critical benchmark for evaluating the performance of any corresponding suboptimal algorithms, such as [8], [10]. Moreover, to strike a balance between performance and complexity, we develop a novel and computationally efficient suboptimal scheme by leveraging successive convex approximation (SCA).
- We introduce a novel CSI error model based on the field response channel model in [7]. Then, building on the framework developed for perfect CSI, we extend our design to the more practical case of imperfect CSI. Specifically, we transform the resulting robust SINR constraints into a set of linear matrix inequality (LMI) constraints. Furthermore, we introduce a set of auxiliary variables to formulate an MINLP problem for robust resource allocation design. Then, we extend the BnB-based and SCA-based methods, originally developed for the case of perfect CSI, to obtain the globally optimal solution and a local optimum for imperfect CSI, respectively.
- By analyzing the convergence behavior of the proposed BnB-based algorithms, we confirm their capability to find global optimal solutions for the considered resource allocation problems for both perfect and imperfect CSI. Furthermore, both proposed SCA-based algorithms achieve local optimality, closely approaching the globally optimal upper bound established by the BnB-based algorithms. Notably, the SCA-based algorithms exhibit a faster convergence, although at the cost of a slightly higher total power consumption compared to the optimal BnB-based algorithms, offering a practical balance between system performance and complexity.

The remainder of this paper is organized as follows: In Section II, we introduce the system model for the considered MA-enabled multi-user multiple-input single-output (MISO) communication system with a spatially discrete transmit area and formulate the corresponding resource allocation problem. In Sections III and IV, the globally optimal and suboptimal solutions for the MA positions and the BS beamformers are developed for perfect and imperfect CSI, respectively. Section V evaluates the performance of the proposed MA-enabled system designs via numerical simulations, and Section VI concludes this paper.

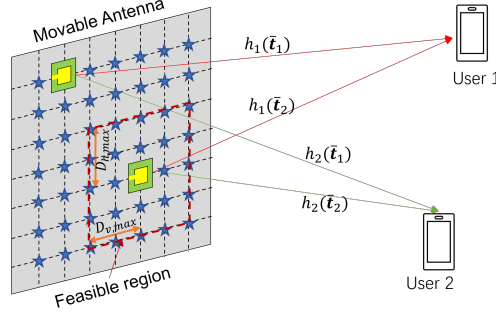


Fig. 1. Transmission from $M = 2$ movable antenna elements with $N = 49$ possible discrete positions to $K = 2$ users (markers “★” indicate discrete antenna positions).

Notation: Vectors and matrices are denoted by boldface lower case and boldface capital letters, respectively. $\mathbb{R}^{N \times M}$ and $\mathbb{C}^{N \times M}$ represent the spaces of $N \times M$ real-valued and complex-valued matrices, respectively. $|\cdot|$ and $\|\cdot\|_2$ stand for the absolute value of a complex scalar and the l_2 -norm of a vector, respectively. $(\cdot)^T$, $(\cdot)^*$, and $(\cdot)^H$ denote the transpose, conjugate, and conjugate transpose of their arguments, respectively. \mathbf{I}_N refers to the identity matrix of dimension N . $\text{Tr}(\cdot)$ is the trace of the input argument. $\mathbf{0}_L$ and $\mathbf{1}_L$ represent the all-zeros and all-ones vector of length L , respectively. $\mathbf{A} \geq \mathbf{0}$ indicates that \mathbf{A} is a positive semidefinite matrix. $\text{diag}(\mathbf{a})$ denotes a diagonal matrix whose main diagonal elements are given by the entries of vector \mathbf{a} . $\text{Re}\{\cdot\}$ and $\text{Im}\{\cdot\}$ represent the real and imaginary parts of a complex number, respectively. $\mathbb{E}[\cdot]$ refers to statistical expectation. The largest eigenvalue of square matrix \mathbf{X} is denoted by $\lambda_{\max}(\mathbf{X})$. $\binom{N}{K}$ denotes the binomial coefficient of the monomial x^K in the expansion of $(1+x)^N$.

II. SYSTEM MODEL

A. System Model

We consider a multi-user wireless communication system where a BS, equipped with M MA elements, serves K single-antenna users in the downlink. The positions of the MA elements can be adjusted simultaneously within a given two-dimensional transmit area. Since practical electro-mechanical devices can only provide horizontal and vertical movement by a fixed constant increment d in each step [13], [14], the transmit area of the MA-enabled communication system is quantized [14]¹. We collect the N possible discrete positions of the MAs in set $\mathcal{P} = \{\mathbf{p}_1, \dots, \mathbf{p}_N\}$, where the distance between neighboring positions is equal to d in horizontal or vertical directions, as shown in Fig. 1. Here, $\mathbf{p}_n = [x_n, y_n]^T$ represents the n -th candidate position with horizontal coordinate x_n and vertical coordinate y_n , $\forall n \in \{1, \dots, N\}$. In other words, the feasible set $\bar{\mathbf{t}}_m$, $\forall m \in \{1, \dots, M\}$, of the position of the m -th MA element is given by \mathcal{P} , i.e., $\bar{\mathbf{t}}_m = [\bar{x}_m, \bar{y}_m]^T \in \mathcal{P}$.

¹The value of step size d depends on the precision of the employed linear actuators of the electro-mechanical devices and may vary in different MA-enabled systems [13], [14].

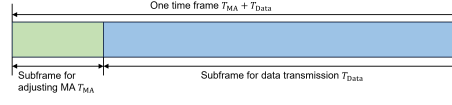


Fig. 2. Time frame structure for the considered quasi-static fading scenario.

In this work, we consider a slow-fading channel and focus on one quasi-static fading block [7], [8], [10]. The slow-varying channel allows moving the MA elements to locations with favorable channel properties at the beginning of each coherence time frame. Hence, as shown in Fig. 2, each coherence time frame is divided into two subframes, where in the first subframe, the MA positions are adjusted while the second subframe is used for data transmission. Here, T_{MA} and T_{Data} denote the time durations of the first and second subframes, respectively. Moreover, the physical channel conditions can be reconfigured by adapting the positions of the MA elements according to the available CSI and the current MA positions. For the sake of notational simplicity, we define $\bar{\mathbf{T}} = [\bar{\mathbf{t}}_1, \dots, \bar{\mathbf{t}}_M] \in \mathbb{R}^{2 \times M}$ as the collection of the positions of all MA elements. Then, the MIMO channel between the BS and the K users is a function of $\bar{\mathbf{T}}$, i.e., $\mathbf{H}(\bar{\mathbf{T}}) = [\mathbf{h}_1(\bar{\mathbf{T}}), \dots, \mathbf{h}_K(\bar{\mathbf{T}})]^H \in \mathbb{C}^{K \times M}$, where $\mathbf{h}_k^H(\bar{\mathbf{T}}) = [h_k(\bar{\mathbf{t}}_1), \dots, h_k(\bar{\mathbf{t}}_M)]$ denotes the channel vector between the BS and the k -th user. Here, $h_k(\bar{\mathbf{t}}_m) \in \mathbb{C}$ represents the channel coefficient between the m -th MA element at position $\bar{\mathbf{t}}_m$ and the k -th user. Therefore, the received signal y_k at the k -th user is given by

$$y_k = \mathbf{h}_k^H(\bar{\mathbf{T}}) \mathbf{w}_k s_k + \sum_{k' \neq k} \mathbf{h}_k^H(\bar{\mathbf{T}}) \mathbf{w}_{k'} s_{k'} + n_k, \quad (1)$$

where $s_k \in \mathbb{C}$ denotes the symbol transmitted to the k -th user and $\mathbb{E}[|s_k|^2] = 1$, $\mathbb{E}[s_k^* s_{k'}] = 0$, $k \neq k'$, $\forall k, k' \in \{1, \dots, K\}$. Here, we define vector $\mathbf{s} = [s_1, \dots, s_K]^T \in \mathbb{C}^{K \times 1}$ to collect the information-carrying symbols transmitted to the users. Vector $\mathbf{w}_k \in \mathbb{C}^{M \times 1}$ is the beamforming vector of the k -th user, and $n_k \in \mathbb{C}$ stands for the additive white Gaussian noise at the k -th user with zero mean and variance σ_k^2 . To simplify the notation, we define sets $\mathcal{K} = \{1, \dots, K\}$ and $\mathcal{M} = \{1, \dots, M\}$ to collect the indices of the users and the MA elements, respectively.

B. Field Response Channel Model

In this work, we adopt the field response channel model proposed in [7] for the considered MA-enabled MISO system. In particular, the channel vector $\mathbf{h}_k(\bar{\mathbf{T}})$ between the BS and the k -th user is contingent upon both the propagation environment and the positions of the M MA elements. Since the size of the transmit area for the MA elements is much smaller than the communication distance between the BS and the users, the far-field condition generally holds for the BS-user channels [7], [8], [10]. Therefore, the field response from the transmit area to the users can be modeled as a plane wave. In particular, adjusting the positions of the MA elements does not impact the angle of departure (AoD), the angle of arrival (AoA), and the amplitude of the multi-path components (MPCs) between the BS and each user, while the phase of the MPCs depends on the MA position.

Without loss of generality, the channel between the BS and the k -th user is assumed to comprise L_k MPCs. Let θ_{k,l_k} and ϕ_{k,l_k} denote the elevation and azimuth AoDs of the l_k -th channel path, $l_k \in \{1, \dots, L_k\}$, of the k -th user, respectively. The transmit field-response vector (FRV) for the channel between the k -th user and an MA element at position \mathbf{p}_n is given as $\mathbf{g}_k(\mathbf{p}_n) = [e^{j\rho_{k,1}(\mathbf{p}_n)}, \dots, e^{j\rho_{k,L_k}(\mathbf{p}_n)}]^T$ [7], where $\rho_{k,l_k}(\mathbf{p}_n) = \frac{2\pi}{\lambda} ((x_k - x_1) \cos \theta_{k,l_k} \sin \phi_{k,l_k} + (y_k - y_1) \sin \theta_{k,l_k})$ represents the phase difference of the l_k -th channel path between \mathbf{p}_n and the reference position, i.e., \mathbf{p}_1 . Here, λ denotes the carrier wavelength. Since the users are equipped with a single antenna, the receive FRV for the k -th user is given by $\mathbf{1}_{L_k}^T$. Thus, the channel coefficient $h_k(\mathbf{p}_n) \in \mathbb{C}$ between an MA element at position \mathbf{p}_n and the k -th user is modeled as follows

$$h_k(\mathbf{p}_n) = \mathbf{1}_{L_k}^T \mathbf{\Psi}_k \mathbf{g}_k(\mathbf{p}_n), \quad (2)$$

where matrix $\mathbf{\Psi}_k = \text{diag}\{\psi_{1,k}, \dots, \psi_{L_k,k}\}^T$, $\psi_{l_k,k} \in \mathbb{C}$, $\forall l_k \in \{1, \dots, L_k\}$, contains the path responses of all L_k channel paths from the transmit area to the k -th user. Moreover, for the sake of presentation, we define an effective channel vector, $\hat{\mathbf{h}}_k \in \mathbb{C}^N$, that collects the channel coefficients between an MA element and the k -th user for all possible $\mathbf{p}_n \in \mathcal{P}$ and is given by

$$\hat{\mathbf{h}}_k = [h_k(\mathbf{p}_1), \dots, h_k(\mathbf{p}_N)]^H = (\mathbf{1}_{L_k}^T \mathbf{\Psi}_k [\mathbf{g}_k(\mathbf{p}_1), \dots, \mathbf{g}_k(\mathbf{p}_N)])^H = \mathbf{G}_k^H \boldsymbol{\psi}_k, \quad (3)$$

where $\mathbf{G}_k = [\mathbf{g}_k(\mathbf{p}_1), \dots, \mathbf{g}_k(\mathbf{p}_N)]$ and $\boldsymbol{\psi}_k = [\psi_{1,k}, \dots, \psi_{L_k,k}]^H$ denote the field response matrix (FPM) and the path response vector of the k -th user, respectively.

C. MA Model

In this paper, we take into account the physical antenna size of the MA elements for MA location design. In particular, two MA elements cannot be placed arbitrarily close to each other to avoid collisions during movement. Thus, the center-to-center distance between any pair of MA elements must exceed a specified minimum distance D_{\min} [8], which is given by

$$\|\bar{\mathbf{t}}_m - \bar{\mathbf{t}}_{m'}\|_2 \geq D_{\min}, m \neq m', \forall m, m' \in \mathcal{M}, \quad (4)$$

where $\bar{\mathbf{t}}_m = [\bar{x}_m, \bar{y}_m]^T$ denotes the position of the m -th MA element.

Furthermore, due to the limitation of electro-mechanical drivers, the moving speed of MA elements is constrained. In this paper, we assume that the adopted MA drivers provide line motion in both horizontal and vertical directions, as shown in [11], [14]. In particular, two motion drivers are deployed for one MA element to enable simultaneous horizontal and vertical motion². For the sake of simplicity, we assume that the horizontal and vertical speeds of the MAs $v_{h,\text{MA}}$ and $v_{v,\text{MA}}$ are constant. Thus, for one transmission block, the maximum horizontal and vertical movement distances of each MA element during the first subframe are limited by $D_{h,\max} = v_{h,\text{MA}} T_{\text{MA}}$ and $D_{v,\max} = v_{v,\text{MA}} T_{\text{MA}}$, respectively, cf. Fig. 1. Therefore,

²The motion control of the MA is similar to the motion control of 3D printers in [19]. Please refer to [19] for more details.

for the considered system, the position of MA element m must satisfy the following constraint:

$$|\bar{x}_m - x_m^0| \leq D_{h,\max}, \quad |\bar{y}_m - y_m^0| \leq D_{v,\max}, \quad (5)$$

where $[x_m^0, y_m^0]$ denote the position of MA element m at the beginning of the first subframe.

In this work, we assume that the power consumptions of the horizontal and vertical MA drivers are constant during MA motion, respectively. Thereby, the energy consumption of the m -th MA driver is proportional to the time interval needed for the horizontal and vertical movement of the m -th MA element, i.e., $t_{m,h,MA} = \frac{|\bar{x}_m - x_m^0|}{v_{h,MA}}$ and $t_{m,v,MA} = \frac{|\bar{y}_m - y_m^0|}{v_{v,MA}}$. The overall energy consumption required for MA motion is given by

$$E_{m,MA} = P_{h,MA} \frac{|\bar{x}_m - x_m^0|}{v_{h,MA}} + P_{v,MA} \frac{|\bar{y}_m - y_m^0|}{v_{v,MA}}, \quad (6)$$

where $P_{h,MA}$ and $P_{v,MA}$ denote the power consumption of the horizontal and vertical MA drivers during movement, respectively.

D. CSI Uncertainty

For optimization of the performance of the considered MA-enabled system, acquiring the CSI of the effective channel vector $\hat{\mathbf{h}}_k$ of the k -th user is essential. However, direct estimation of $\hat{\mathbf{h}}_k$ may not be feasible due to the limited number of antenna elements. Meanwhile, compressive sensing-based (CS-based) methods are advocated in [15], [16] to estimate the MA channels by exploiting the sparse representation of the channel responses in $\hat{\mathbf{h}}_k$ in terms of the MPCs. In particular, the CS-based methods in [15], [16] first estimate the FPM \mathbf{G}_k , and then the path response vector ψ_k to reconstruct the effective channel vector $\hat{\mathbf{h}}_k$ of the k -th user. Thanks to the assumed quasi-static environment, the FPMs of all users can be regarded as constant and can be accurately estimated at the BS [16]. On the other hand, the path response vector is recovered by CS-based methods such as the orthogonal matching pursuit algorithm, which only guarantees accurate estimation of the dominant paths [15], [16]. Therefore, CS-based methods introduce CSI estimation errors in the recovered path response vector. In this work, we adopt a norm-bounded error model for the path response vector. Specifically, the effective channel vector $\hat{\mathbf{h}}_k$ between the MA region and the k -th user is modeled as follows

$$\hat{\mathbf{h}}_k = \mathbf{G}_k(\bar{\psi}_k + \Delta\psi_k), \quad \Omega_{\Delta\psi_k} = \{\Delta\psi_k \in \mathbb{C}^{L_k} : \|\Delta\psi_k\|_2^2 \leq \epsilon_k^2\}, \quad \forall k, \quad (7)$$

where $\bar{\psi}_k$ and $\Delta\psi_k$ denote the estimate and the estimation error of the path response vector of the k -th user, respectively. Furthermore, the norm of the CSI error, $\Delta\psi_k$, is bounded by constant ϵ_k^2 and set $\Omega_{\Delta\psi_k}$ contains all possible CSI errors satisfying the bounded norm condition.

III. ALGORITHM DESIGN FOR PERFECT CSI

In this section, assuming perfect CSI is available at the BS, we first formulate the resource allocation problem for the considered MA-enabled systems and transform it into a more tractable MINLP problem.

Then, we develop two algorithms based on the BnB and SCA methods to attain the global optimum and a local optimum of the reformulated MINLP problem, respectively.

A. Problem Formulation

In this section, we formulate the proposed resource allocation problem for the considered system. We first rewrite $\mathbf{h}_k^H(\bar{\mathbf{T}})$ as follows

$$\mathbf{h}_k^H(\bar{\mathbf{T}}) = \hat{\mathbf{h}}_k^H \mathbf{B}, \quad (8)$$

where $\mathbf{B} = [\mathbf{b}_1, \dots, \mathbf{b}_M]$ and $\mathbf{b}_m = [b_m[1], \dots, b_m[N]]^T$ denotes the binary selection vector of the m -th MA element. Here, $b_m[n] \in \{0, 1\}$ with $\sum_{n=1}^N b_m[n] = 1$ is a binary variable defining the position of the m -th MA element. Note that $b_m[n] = 1$ if and only if the n -th MA position in \mathcal{P} is selected, i.e., $\bar{\mathbf{t}}_m = \mathbf{p}_n$. Thus, the received signal of the k -th user is given by

$$y_k = \hat{\mathbf{h}}_k^T \mathbf{B} \sum_{k \in \mathcal{K}} \mathbf{w}_k s_k + n_k = \hat{\mathbf{h}}_k^T \mathbf{B} \mathbf{W} \mathbf{s} + n_k, \quad (9)$$

where $\mathbf{W} = [\mathbf{w}_1, \dots, \mathbf{w}_K]$ denotes the collection of the beamforming vectors of all users. Therefore, the received SINR of the k -th user is given by

$$\text{SINR}_k = \frac{|\hat{\mathbf{h}}_k^H \mathbf{B} \mathbf{w}_k|^2}{\sum_{k' \in \mathcal{K}, k' \neq k} |\hat{\mathbf{h}}_k^H \mathbf{B} \mathbf{w}_{k'}|^2 + \sigma_k^2}. \quad (10)$$

Next, we define distance matrix $\mathbf{D} \in \mathbb{C}^{N \times N}$, where element $D_{n,n'}$ in the n -th row and n' -th column of \mathbf{D} denotes the distance between the n -th and the n' -th candidate positions in \mathcal{P} . Thus, the minimum distance constraint between any pair of MA elements in (4) can be reformulated as

$$\mathbf{b}_m^T \mathbf{D} \mathbf{b}_{m'} \geq D_{\min}, \quad m \neq m', \quad \forall m, m' \in \mathcal{M}. \quad (11)$$

Moreover, let vector $\mathbf{d}_{h,m} = [|x_1 - x_m^0|, \dots, |x_N - x_m^0|]$ and $\mathbf{d}_{v,m} = [|y_1 - y_m^0|, \dots, |y_N - y_m^0|]$ collect the horizontal and vertical distances between all candidate positions in \mathcal{P} and the initial position of MA element m . Then, the maximal moving distance constraints in (5) can be equivalently rewritten as

$$\mathbf{b}_m^T \mathbf{d}_{h,m} \leq D_{h,\max}, \quad \mathbf{b}_m^T \mathbf{d}_{v,m} \leq D_{v,\max}, \quad \forall m \in \mathcal{M}. \quad (12)$$

In the considered MA-enabled MISO system, the BS energy consumption comprises the energy consumed by the MA drivers, and the energy radiated for data transmission. Thus, the total energy consumption at the BS, E_{total} , is given by

$$E_{\text{total}} = \sum_{m \in \mathcal{M}} E_{m,\text{MA}} + \sum_{k \in \mathcal{K}} \|\mathbf{w}_k\|_2^2 T_{\text{Data}}. \quad (13)$$

Next, we define the energy consumption vector of the m -th MA element $\mathbf{e}_m \in \mathbb{C}^N$ as $\mathbf{e}_m = [e_{m,1}, \dots, e_{m,N}]^T$, where $e_{m,n} = P_{\text{MA}} \frac{|x_n - x_m^0| + |y_n - y_m^0|}{v_{\text{MA}}}$. Then, the total energy consumption E_{total} and the average power consumption \bar{P} at the BS can be rewritten as

$$E_{\text{total}} = \sum_{m \in \mathcal{M}} \mathbf{b}_m^T \mathbf{e}_m + \sum_{k \in \mathcal{K}} \|\mathbf{w}_k\|_2^2 T_{\text{Data}}, \quad (14)$$

and

$$\bar{P}(\mathbf{W}, \mathbf{B}) = \frac{E_{\text{total}}}{T_{\text{MA}} + T_{\text{Data}}}, \quad (15)$$

respectively. In this paper, we aim to minimize the BS's power consumption within one transmission block while guaranteeing a minimum required SINR for each user. The resulting resource allocation problem can be formulated as follows

$$\begin{aligned}
& \underset{\mathbf{W}, \mathbf{B}}{\text{minimize}} \quad \bar{P}(\mathbf{W}, \mathbf{B}) \\
& \text{s.t.} \quad \text{C1: } \text{SINR}_k \geq \gamma_k, \quad \forall k \in \mathcal{K}, \\
& \quad \text{C2: } \mathbf{b}_m^T \mathbf{D} \mathbf{b}_{m'} \geq D_{\min}, \quad m \neq m', \quad \forall m, m' \in \mathcal{M}, \\
& \quad \text{C3: } \mathbf{b}_m^T \mathbf{d}_{h,m} \leq D_{h,\max}, \quad \mathbf{b}_m^T \mathbf{d}_{v,m} \leq D_{v,\max}, \quad \forall m \in \mathcal{M}, \\
& \quad \text{C4: } b_m[n] \in \{0, 1\}, \quad \forall n \in \mathcal{N}, \forall m \in \mathcal{M}, \\
& \quad \text{C5: } \sum_{n \in \mathcal{N}} b_m[n] = 1, \quad \forall m \in \mathcal{M},
\end{aligned} \tag{16}$$

where $\gamma_k \geq 0$ in constraint C1 denotes the pre-defined minimum required SINR of the k -th user. Note that the above optimization problem is non-convex due to the coupling between \mathbf{W} and \mathbf{B} in constraint C1 and binary constraint C4. In fact, the optimization problem in (16) is a combinatorial optimization problem which is generally NP-hard [20]–[22]. In the following, we develop a BnB-based iterative algorithm to obtain the global optimum of (16).

B. Problem Transformation

By introducing an auxiliary matrix $\mathbf{X} = \mathbf{B}\mathbf{W}$, $\mathbf{X} \in \mathbb{C}^{N \times K}$, the received signal of the k -th user can be rewritten as follows

$$y_k = \hat{\mathbf{h}}_k^H \mathbf{X} \mathbf{s} + n_k. \tag{17}$$

Thus, we can recast the SINR of the k -th user as

$$\text{SINR}_k = \frac{|\hat{\mathbf{h}}_k^H \mathbf{x}_k|^2}{\sum_{k' \in \mathcal{K} \setminus \{k\}} |\hat{\mathbf{h}}_k^H \mathbf{x}_{k'}|^2 + \sigma_k^2}, \tag{18}$$

where \mathbf{x}_k denotes the k -th column of \mathbf{X} . Then, by exploiting (18) in constraint C1, problem (16) can be equivalently reformulated as follows

$$\begin{aligned}
& \underset{\mathbf{B}, \mathbf{W}, \mathbf{X}}{\text{minimize}} \quad \bar{P}(\mathbf{W}, \mathbf{B}) \\
& \text{s.t.} \quad \text{C1, C2, C3, C4, C5, C6: } \mathbf{X} = \mathbf{B}\mathbf{W}.
\end{aligned} \tag{19}$$

Note that equality constraint C6 is non-convex due to the coupling between \mathbf{B} and \mathbf{W} . To tackle this non-convexity, we present the following Lemma to reformulate constraint C6 into two equivalent convex constraints.

Lemma 1. *Equality constraint C6 is equivalent to the following linear matrix inequality (LMI) constraints,*

$$\text{C6a: } \begin{bmatrix} \mathbf{U} & \mathbf{X} & \mathbf{B} \\ \mathbf{X}^H & \mathbf{V} & \mathbf{W}^H \\ \mathbf{B}^H & \mathbf{W} & \mathbf{I}_M \end{bmatrix} \succeq \mathbf{0}, \quad \text{C6b: } \text{Tr}(\mathbf{U}) - M \leq 0, \tag{20}$$

where $\mathbf{U} \in \mathbb{C}^{N \times N}$ and $\mathbf{V} \in \mathbb{C}^{K \times K}$ are two auxiliary optimization variables with $\mathbf{U} \succeq \mathbf{0}$ and $\mathbf{V} \succeq \mathbf{0}$.

Proof. Please refer to Appendix A. □

On the other hand, minimum distance constraint C2 is also non-convex. Therefore, we exploit the following lemma to convexify constraint C2 based on the binary nature of matrix \mathbf{B} .

Lemma 2. Let $\bar{\mathbf{b}} = [\mathbf{b}_1^T, \dots, \mathbf{b}_M^T]^T$ denote a binary vector collecting all binary selection vectors \mathbf{b}_m , $\forall m$. Inequality constraint C2 is equivalent to the following quadratic inequality constraint

$$\overline{\text{C2}} : \bar{\mathbf{b}}^T \left(\frac{-\mathbf{D}_{m,m'} - \mathbf{D}_{m,m'}^T}{2} + \eta \mathbf{I}_{MN} \right) \bar{\mathbf{b}} - \eta M + D_{\min} \leq 0, \quad m \neq m', \quad \forall m, m' \in \mathcal{M}, \quad (21)$$

where $\eta \in \mathbb{R}_+$ is an arbitrary real positive number, $\mathbf{D}_{m,m'} = \hat{\mathbf{I}}_m^T \mathbf{D} \hat{\mathbf{I}}_{m'}$, and $\hat{\mathbf{I}}_m = [\mathbf{0}_{N \times (m-1)N}, \mathbf{I}_N, \mathbf{0}_{N \times (M-m)N}]$.

Proof. Please refer to Appendix B. □

Note that $\overline{\text{C2}}$ is convex for all real values $\eta \geq \lambda_{\max}(\frac{\mathbf{D}_{m,m'} + \mathbf{D}_{m,m'}^T}{2})$. In addition, we observe that SINR constraint C1 is non-convex as well. However, if an arbitrary \mathbf{x}_k satisfies the constraints in (16), \mathbf{x}_k multiplied by an arbitrary phase shift $e^{j\phi}$ also satisfies the constraints without affecting the value of the objective function. Thus, we can leverage the following lemma to transform the non-convex SINR constraint in C1 into two equivalent convex constraints, cf. also [23], [24].

Lemma 3. Without loss of optimality, we assume that $\hat{\mathbf{h}}_k^H \mathbf{x}_k \in \mathbb{R}$. Then, constraint C1 can be equivalently rewritten as

$$\text{C1a: } \sqrt{\sum_{k' \in \mathcal{K} \setminus \{k\}} |\hat{\mathbf{h}}_k^H \mathbf{x}_{k'}|^2 + \sigma_k^2} - \frac{\text{Re}\{\hat{\mathbf{h}}_k^H \mathbf{x}_k\}}{\sqrt{\gamma_k}} \leq 0, \quad \forall k \in \mathcal{K}, \quad (22)$$

$$\text{C1b: } \text{Im}\{\hat{\mathbf{h}}_k^H \mathbf{x}_k\} = 0, \quad \forall k \in \mathcal{K}. \quad (23)$$

C1a and C1b are both convex constraints.

Proof. Please refer to [23, Section III]. □

Thus, the resource allocation optimization problem in (16) can be equivalently reformulated as follows

$$\begin{aligned} & \underset{\mathbf{X}, \mathbf{W}, \mathbf{B}, \mathbf{U}, \mathbf{V}}{\text{minimize}} && \bar{P}(\mathbf{W}, \mathbf{B}) \\ & \text{s.t.} && \text{C1a, C1b, } \overline{\text{C2}}, \text{C3, C4, C5, C6a, C6b.} \end{aligned} \quad (24)$$

Note that the optimization problem in (24) is an MINLP problem, where C4 is the only non-convex constraint. Thus, if we employ linear relaxation to constraint C4, the optimization problem becomes a convex optimization problem with respect to \mathbf{X} , \mathbf{W} , \mathbf{U} , \mathbf{V} , and \mathbf{B} , and can be optimally solved by numerical solvers such as CVX [25]. On the other hand, for a given fixed binary matrix \mathbf{B} , the MINLP problem in (24) degenerates into a convex optimization problem with respect to variables \mathbf{X} , \mathbf{W} , \mathbf{U} and \mathbf{V} . Thus, rigorous lower and upper bounds of the problem over any given variable subdomain can be generated. In particular, a feasible upper bound is obtained by solving (24) for a given feasible \mathbf{B} , while a lower bound is obtained

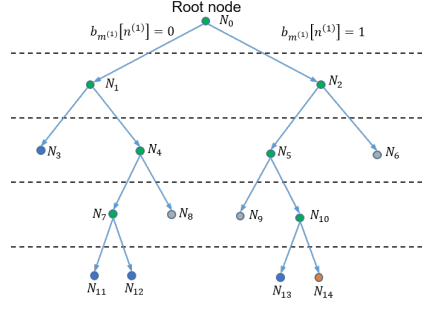


Fig. 3. An illustration of the BnB tree for $M = 2$ and $N = 2$ in the 7-th iteration. The green, blue, grey, and orange dots correspond to internal, external, discarded, and optimal nodes, respectively.

from convex relaxations of binary constraint C4. Therefore, the BnB method can be exploited to obtain the optimal solution of the MINLP problem in (24) [26], [27].

C. Proposed BnB-based Algorithm

We develop an iterative algorithm based on the BnB method to optimally solve the MINLP problem in (24). The crux of the BnB method is to divide the feasible region into partitions arranged in a tree structure, with the feasible set of the main problem mapped to the root of the tree. Each node of the BnB tree represents a subset of the solution set. By subdividing the feasible region into a series of subsets, the problem in (24) is decomposed into manageable smaller subproblems corresponding to the subsets. In particular, for each subproblems, a lower- and an upper-bound solution are constructed. Specifically, these bounds are exploited to eliminate any subsets that cannot possibly contain the optimal solution. In particular, a subset is discarded if it cannot produce a better solution than the current best solution found by the algorithm, i.e., if the lower bound for this subset is larger than the current global upper bound across all subsets. As the iterative BnB algorithm progresses, non-optimal subsets are discarded, and based on a predefined node selection strategy, one node in the current BnB tree is selected and branched into two new nodes in each iteration. With the expansion of the BnB tree, the feasible set is progressively partitioned into smaller subsets with more accurate lower and upper bounds. Following the above procedure, the gap between the upper bound and the lower bound gradually diminishes with each iteration and the BnB-based algorithm converges towards the global optimum of the considered optimization problem. In the following, we present the proposed BnB-based algorithm in detail.

1) *Initialization:* We first initialize the BnB tree $\mathcal{T}^{(0)} = \{\mathcal{N}_0\}$, where $\mathcal{N}_0 = \{\mathcal{B}^{(0)}, F_L^{(0)}, F_U^{(0)}\}$ denotes the root node of $\mathcal{T}^{(0)}$. The search space $\mathcal{B}^{(0)}$ of the binary matrix \mathbf{B} corresponding to the root node of the BnB tree is the product of $M \times N$ binary sets, i.e., $\mathcal{B}^{(0)} = \prod_{(m,n) \in \mathcal{L}} \mathcal{B}_{m,n}^{(0)}$, where $\mathcal{L} = \{(1, 1), \dots, (M, N)\}$ denotes the collection of all (m, n) pairs, and $\mathcal{B}_{m,n}^{(0)} = \{0, 1\}, \forall m, n$, denote the feasible set of binary variable $b_m[n]$. Moreover, $F_L^{(0)}$ and $F_U^{(0)}$ denote the lower and upper bounds for (24) in search space $\mathcal{B}^{(0)}$, respectively.

To obtain an initial lower bound for (24), we relax the discrete search space $\mathcal{B}^{(0)}$ into a continuous space $\tilde{\mathcal{B}}^{(0)} = \prod_{(m,n) \in \mathcal{L}} \tilde{\mathcal{B}}_{m,n}^{(0)}$, where $\tilde{\mathcal{B}}_{m,n}^{(0)} = \{b_m[n] \mid 0 \leq b_m[n] \leq 1\}$ denotes the relaxed continuous set of $\mathcal{B}_{m,n}^{(0)}$. Then, the lower bound $F_L^{(0)}$ for (24) is obtained by solving

$$\begin{aligned} & \underset{\mathbf{X}, \mathbf{W}, \mathbf{B}, \mathbf{U}, \mathbf{V}}{\text{minimize}} \quad \bar{P}(\mathbf{W}, \mathbf{B}) \\ & \text{s.t.} \quad \text{C1a, C1b, } \overline{\text{C2}}, \text{C3, C5, C6a, C6b, } \overline{\text{C4}} : \mathbf{B} \in \tilde{\mathcal{B}}^{(0)}, \end{aligned} \quad (25)$$

which is a convex optimization problem and can be optimally solved by existing numerical convex programming solvers, e.g., CVX [25]. The optimal solutions of \mathbf{B} and \mathbf{W} obtained from (25) are denoted as $\mathbf{B}_L^{(0)} = [\mathbf{b}_{L,1}^{(0)}, \dots, \mathbf{b}_{L,M}^{(0)}]$ and $\mathbf{W}_L^{(0)} = [\mathbf{w}_{L,1}^{(0)}, \dots, \mathbf{w}_{L,K}^{(0)}]$, respectively. We note that the optimal $\mathbf{B}_L^{(0)}$ may be non-binary since the original binary constraint has been relaxed. Thus, the solution of the relaxed problem in (25) establishes a lower bound for (24), which is given by $F_L^{(0)} = \bar{P}(\mathbf{W}_L^{(0)}, \mathbf{B}_L^{(0)})$. On the other hand, we can obtain an initial upper bound for (24) based on the solution of (25). In particular, based on $\mathbf{B}_L^{(0)}$, we construct a binary solution $\mathbf{B}_U^{(0)}$ that has minimum Euclidean distance to $\mathbf{B}_L^{(0)}$ by solving the following optimization problem

$$\begin{aligned} & \underset{\mathbf{B}}{\text{minimize}} \quad \|\mathbf{B} - \mathbf{B}_L^{(0)}\|_F \\ & \text{s.t.} \quad \overline{\text{C2}}, \text{C3, C4, C5}, \end{aligned} \quad (26)$$

which is non-convex due to binary constraint C4. To circumvent this difficulty, we recast C4 equivalently in form of the following inequality constraint and $\overline{\text{C4}}$

$$\text{C4a} : \sum_{m=1}^M \sum_{n=1}^N (b_m[n] - b_m^2[n]) \leq 0, \quad (27)$$

where constraint C4a is a difference of convex (DC) functions [28]. To facilitate low-complexity algorithm design, we resort to the penalty-based method [29] to tackle DC constraint C4a and rewrite the problem in (26) as follows

$$\begin{aligned} & \underset{\mathbf{B}}{\text{minimize}} \quad \|\mathbf{B} - \mathbf{B}_L^{(0)}\|_F + \frac{1}{\mu} \sum_{m=1}^M \sum_{n=1}^N (b_m[n] - b_m^2[n]) \\ & \text{s.t.} \quad \overline{\text{C2}}, \text{C3, C4b, C5}, \end{aligned} \quad (28)$$

where $\mu > 0$ is a penalty factor for penalizing the violation of the binary constraint. When μ is sufficiently small, i.e., $\mu \rightarrow 0$, problem (26) and problem (28) are equivalent [28]. Now, the objective function in (26) is in the canonical form of a DC problem. Hence, a suboptimal solution of (28) can be obtained by the SCA method [28]. In particular, in the $(j+1)$ -th iteration of the SCA algorithm, we construct a global underestimator for the term $\sum_{m=1}^M \sum_{n=1}^N b_m^2[n]$ by leveraging first-order Taylor approximation as follows:

$$\sum_{m=1}^M \sum_{n=1}^N b_m^2[n] \geq \sum_{m=1}^M \sum_{n=1}^N 2b_m^{(j)}[n]b_m[n] - (b_m^{(j)}[n])^2, \quad (29)$$

where $b_m^{(j)}[n]$ is the solution for $b_m[n]$ in the j -th iteration. As a result, the optimization problem in the j -th iteration of the SCA algorithm is given by

$$\underset{\mathbf{B}}{\text{minimize}} \quad \|\mathbf{B} - \mathbf{B}_L^{(0)}\|_F + \frac{1}{\mu}$$

Algorithm 1 SCA Algorithm

1: Set iteration index $j = 0$ and set $\mathbf{B}^{(0)}$. Set convergence tolerance $0 < \Delta_{\text{SCA}} \ll 1$ and penalty factor $0 < \mu \ll 1$.

2: **repeat**

3: Set $j = j + 1$.

4: Solve (30) for given $\mathbf{B}^{(j-1)}$ and update $\mathbf{B}^{(j)}$ as the optimal solution of (30).

5: **until** $\frac{\|\mathbf{B}^{(j-1)} - \mathbf{B}^{(j)}\|_F}{\|\mathbf{B}^{(j-1)}\|_F} \leq \Delta_{\text{SCA}}$

$$\begin{aligned} & \sum_m \sum_n (b_m[n] - 2b_m^{(j)}[n]b_m[n] - (b_m^{(j)}[n])^2) \\ \text{s.t.} \quad & \overline{\text{C2}}, \text{C3}, \overline{\text{C4}}, \text{C5}. \end{aligned} \quad (30)$$

The problem in (30) is convex and can be optimally solved by CVX. The proposed iterative SCA algorithm to obtain $\mathbf{B}_U^{(0)}$ is summarized in **Algorithm 1**. The proposed algorithm can obtain a suboptimal binary solution of (26). An upper bound of (24) can be generated based on any feasible \mathbf{B} satisfying constraints $\overline{\text{C2}}, \text{C3}, \overline{\text{C4}}, \text{C5}$ [27]. Thus, based on the binary solution $\mathbf{B}_U^{(0)}$, an upper bound for (24) is obtained by solving the optimization problem in (25) for fixed $\mathbf{B} = \mathbf{B}_U^{(0)}$, e.g., by using again CVX [25]. Here, $\mathbf{W}_U^{(0)} = [\mathbf{w}_{U,1}^{(0)}, \dots, \mathbf{w}_{U,K}^{(0)}]$ denotes the optimal \mathbf{W} obtained by solving (25) with fixed $\mathbf{B} = \mathbf{B}_U^{(0)}$. Then, an initial upper bound of (24) is given by $F_U^{(0)} = \bar{P}(\mathbf{W}_U^{(0)}, \mathbf{B}_U^{(0)})$.

2) *Branch and Bound*: At the beginning of the t -th iteration, the BnB tree obtained in the last iteration is given by $\mathcal{T}^{(t-1)}$. Here, we let sets $\mathcal{I}^{(t-1)}$ and $\mathcal{E}^{(t-1)}$ denote the collections of internal and external nodes of the BnB tree $\mathcal{T}^{(t-1)}$, respectively, as shown in Fig. 3. Here, internal and external nodes represent the nodes with and without child nodes, respectively. Then, we select the node $\mathcal{N}_{i_t} = \{\mathcal{B}^{(i_t)}, F_L^{(i_t)}, F_U^{(i_t)}\}$, $\mathcal{N}_{i_t} \in \mathcal{E}^{(t-1)}$, from the external nodes of the BnB tree $\mathcal{T}^{(t-1)}$ with the smallest lower bound $F_L^{(i_t)}$, where i_t denotes the index of the selected node. Here, $\mathcal{B}^{(i_t)} = \prod_{(m,n) \in \mathcal{L}} \mathcal{B}_{m,n}^{(i_t)}$ denotes the search space of \mathbf{B} corresponding to the selected node \mathcal{N}_{i_t} . In particular, $\mathcal{B}^{(i_t)}$ contains binary sets corresponding to the undetermined binary optimization variables to be optimized in future iterations, i.e., $\mathcal{B}_{m,n}^{(i_t)} = \{0, 1\}$, and determined binary variables, i.e., $\mathcal{B}_{m,n}^{(i_t)} = \{0\}$ or $\{1\}$. We let set $\mathcal{U}^{(i_t)}$ and $\mathcal{D}^{(i_t)}$ collect the indices of undetermined and determined binary variables, respectively.

Then, we partition the selected node \mathcal{N}_{i_t} into two child nodes based on the Euclidean distance between $\mathbf{B}_L^{(i_t)}$ and $\mathbf{B}_U^{(i_t)}$, which are the solutions of \mathbf{B} corresponding to lower and upper bounds $F_L^{(i_t)}$ and $F_U^{(i_t)}$, respectively. In particular, we find the undetermined binary variable $b_{m^{(t)}}[n^{(t)}]$ with index $(m^{(t)}, n^{(t)}) \in \mathcal{U}^{(i_t)}$, where $(m^{(t)}, n^{(t)})$ is given by

$$(m^{(t)}, n^{(t)}) = \arg \max_{(m,n) \in \mathcal{U}^{(i_t)}} |b_{L,m}^{(i_t)}[n] - b_{U,m}^{(i_t)}[n]|, \quad (31)$$

where $b_{L,m}^{(i_t)}[n]$ and $b_{U,m}^{(i_t)}[n]$ denote the n -th element in the m -th column of $\mathbf{B}_L^{(i_t)}$ and $\mathbf{B}_U^{(i_t)}$, respectively. Then, the feasible set of $b_{m^{(t)}}[n^{(t)}]$, i.e., $\mathcal{B}_{m^{(t)},n^{(t)}}^{(i_t)}$ is divided into two subsets $(\mathcal{B}_{m^{(t)},n^{(t)}}^{(i_t)})_0 = \{0\}$ and $(\mathcal{B}_{m^{(t)},n^{(t)}}^{(i_t)})_1 = \{1\}$. In the t -th iteration, resource allocation problems $\mathcal{P}_i, i \in \{0, 1\}$, corresponding to the two child nodes

are given by

$$\begin{aligned} \mathcal{P}_i : \quad & \underset{\mathbf{X}, \mathbf{W}, \mathbf{B}, \mathbf{U}, \mathbf{V}}{\text{minimize}} \quad \bar{P}(\mathbf{W}, \mathbf{B}) \\ \text{s.t.} \quad & \text{C1a, C1b, } \overline{\text{C2}}, \text{C3, C5, C6a, C6b,} \\ & \widetilde{\text{C4a}} : b_m[n] \in \mathcal{B}_{m,n}^{(i_t)}, \forall (m, n) \in \mathcal{L} \setminus (m^{(t)}, n^{(t)}), \widetilde{\text{C4b}} : b_{m^{(t)}}[n^{(t)}] = i. \end{aligned} \quad (32)$$

Note that constraint $\widetilde{\text{C4a}}$ is non-convex since it contains undetermined binary variables $b_m[n]$ to be optimized in future iterations. Similar to the procedure for deriving the initial upper bound, we relax the feasible set of the undetermined binary variables $b_m[n]$ into the corresponding convex hull, i.e., $\widetilde{\mathcal{B}}_{m,n}^{(i_t)} = \{b_m[n] \mid 0 \leq b_m[n] \leq 1\}$, $\forall (m, n) \in \mathcal{U}^{(i_t)} \setminus (m^{(t)}, n^{(t)})$. Then, the lower bound of (32) is obtained by solving the following relaxed optimization problems $\tilde{\mathcal{P}}_i$, $i \in \{0, 1\}$

$$\begin{aligned} \tilde{\mathcal{P}}_i : \quad & \underset{\mathbf{X}, \mathbf{W}, \mathbf{B}, \mathbf{U}, \mathbf{V}}{\text{minimize}} \quad \bar{P}(\mathbf{W}, \mathbf{B}) \\ \text{s.t.} \quad & \text{C1a, C1b, } \overline{\text{C2}}, \text{C3, } \widetilde{\text{C4b}}, \text{C5, C6a, C6b,} \\ & \widetilde{\text{C4c}} : b_m[n] \in \mathcal{B}_{m,n}^{(i_t)}, \forall (m, n) \in \mathcal{D}^{(i_t)}, \\ & \widetilde{\text{C4d}} : 0 \leq b_m[n] \leq 1, \forall (m, n) \in \mathcal{U}^{(i_t)} \setminus (m^{(t)}, n^{(t)}) \end{aligned} \quad (33)$$

Note that $\tilde{\mathcal{P}}_i$ is a convex optimization problem and can be optimally solved by CVX. Here, the optimal solutions of relaxed optimization problems $\tilde{\mathcal{P}}_0$ and $\tilde{\mathcal{P}}_1$ are denoted as $(\mathbf{B}_{L,0}^{(t)}, \mathbf{W}_{L,0}^{(t)})$ and $(\mathbf{B}_{L,1}^{(t)}, \mathbf{W}_{L,1}^{(t)})$, respectively. Then, the lower bounds of problems $\tilde{\mathcal{P}}_0$ and $\tilde{\mathcal{P}}_1$ are given by the objective function values $F_{L,0}^{(t)} = \bar{P}(\mathbf{W}_{L,0}^{(t)}, \mathbf{B}_{L,0}^{(t)})$ and $F_{L,1}^{(t)} = \bar{P}(\mathbf{W}_{L,1}^{(t)}, \mathbf{B}_{L,1}^{(t)})$, respectively.

On the other hand, based on the optimal solutions $\mathbf{B}_{L,0}^{(t)}$ and $\mathbf{B}_{L,1}^{(t)}$ of the relaxed problems, we can obtain the corresponding binary solution $\mathbf{B}_{U,0}^{(t)}$ and $\mathbf{B}_{U,1}^{(t)}$ based on **Algorithm 1**. Subsequently, we solve the problem in (32) by fixing the binary solutions $\mathbf{B} = \mathbf{B}_{U,0}^{(t)}$ and $\mathbf{B} = \mathbf{B}_{U,1}^{(t)}$ and obtain the corresponding upper bounds $F_{U,0}^{(t)}$ and $F_{U,1}^{(t)}$, respectively. After deriving these lower and upper bounds, we expand the BnB tree $\mathcal{T}^{(t-1)}$ by introducing two new child nodes of the selected node \mathcal{N}_{i_t} corresponding to $b_{m^{(t)}}[n^{(t)}] = 0$ and $b_{m^{(t)}}[n^{(t)}] = 1$, respectively. Let $\mathcal{T}^{(t)}$ denote the BnB tree after introducing the new child nodes. Then, the global lower and upper bounds in the t -th iteration, i.e., $\text{LB}^{(t)}$ and $\text{UB}^{(t)}$, are given by the smallest lower and upper bound among all external nodes in $\mathcal{T}^{(t)}$. At the end of one iteration, the search tree is pruned by discarding the nodes whose lower bounds are worse than the current upper bound, as shown in Fig. 3.

3) *Overall Algorithm* The complete BnB procedure is outlined in **Algorithm 2**. Some additional remarks are as follows:

- *Optimality and convergence:* The set partitioning, node branching, and bound update steps are iteratively performed to reduce the difference between the lower and upper bounds. According to [26], the proposed BnB-based algorithm is guaranteed to converge within a finite number of iterations to an ϵ -optimal solution for a given convergence tolerance $\Delta_{\text{BnB}} \geq 0$
- *Complexity:* In each iteration of **Algorithm 2**, we add two new nodes to the BnB tree. For each new

Algorithm 2 Optimal Resource Allocation Algorithm for Perfect CSI

- 1: Solve problem in (25) to obtain optimal solutions $\mathbf{B}_L^{(0)}$ and $\mathbf{W}_L^{(0)}$. Initialize lower bound $\text{LB} = F_L^{(0)}$.
 - 2: Compute the binary solution $\mathbf{B}_U^{(0)}$ according to **Algorithm 1** and obtain the upper bound $\text{UB} = F_U^{(0)}$ by solving problem in (25) for fixed $\mathbf{B} = \mathbf{B}_U^{(0)}$.
 - 3: Initialize BnB tree $\mathcal{T}^{(0)} = \{\mathcal{N}_0\}$. Set convergence tolerance $0 \leq \Delta_{\text{BnB}}$ and iteration index $t = 0$.
 - 4: **repeat**
 - 5: $t = t + 1$,
 - 6: Select the external node \mathcal{N}_{i_t} with the smallest lower bound.
 - 7: Obtain the branching index $(m^{(t)}, n^{(t)})$. Divide feasible set $\mathcal{B}^{(i_t)}$ into two subsets corresponding to $b_{m^{(t)}}[n^{(t)}] = 0$ and $b_{m^{(t)}}[n^{(t)}] = 1$, respectively.
 - 8: Solve the relaxed version of the two subproblems \mathcal{P}_0 and \mathcal{P}_1 in (32) to obtain the optimal solutions $(\mathbf{B}_{L,0}^{(t)}, \mathbf{W}_{L,0}^{(t)})$ and $(\mathbf{B}_{L,1}^{(t)}, \mathbf{W}_{L,1}^{(t)})$, respectively. Store the corresponding lower bounds $F_{L,0}^{(t)}$ and $F_{L,1}^{(t)}$.
 - 9: Compute the binary solution $\mathbf{B}_{U,0}^{(t)}$ and $\mathbf{B}_{U,1}^{(t)}$ based on $\mathbf{B}_{L,0}^{(t)}$ and $\mathbf{B}_{L,1}^{(t)}$, respectively.
 - 10: Solve the problem in (32) by fixing $\mathbf{B} = \mathbf{B}_{U,0}^{(t)}$ and $\mathbf{B} = \mathbf{B}_{U,1}^{(t)}$. Store the upper bounds $F_{U,0}^{(t)}$ and $F_{U,1}^{(t)}$.
 - 11: Expand the tree by adding the two child nodes corresponding to $b_{m^{(t)}}[n^{(t)}] = 0$ and $b_{m^{(t)}}[n^{(t)}] = 1$ for the selected node \mathcal{N}_{i_t} .
 - 12: Update $\text{LB}^{(t)}$ and $\text{UB}^{(t)}$ as the smallest lower bound and upper bound among the external nodes in the tree.
 - 13: **until** $\text{UB}^{(t)} - \text{LB}^{(t)} \leq \Delta_{\text{BnB}}$
-

node, we have to solve two convex optimization problems to obtain the corresponding lower and upper bounds, respectively. In particular, the optimization problems for computing the upper and lower bounds involve one semidefinite programming (SDP) constraint with dimension $\mathcal{O}(N + M + K)$. Therefore, the computational complexity of solving the optimization problems for the lower and upper bounds in each iteration is given by $\mathcal{O}(\log \frac{1}{\rho}((N + M + K)^3 + (N + M + K)^2))$, where $\mathcal{O}(\cdot)$ is the big-O notation, and $\rho > 0$ is the convergence tolerance of the interior point method that is implemented in CVX [30, Theorem 3.12]. We note that our simulation results in Section V reveal the proposed BnB-based algorithm exhibits a considerably faster convergence rate than an exhaustive search, even though the worst-case computational complexity of BnB algorithms scales exponentially with the number of MA elements [26].

D. Proposed SCA-based Algorithm

To strike a balance between complexity and optimality, we develop a suboptimal SCA-based algorithm with reduced complexity. Following a similar procedure as in Section III-C for deriving the initial upper bound, we recast binary constraint C4 as the two convex inequality constraints, $\overline{\text{C4}}$ and C4a. Then, we resort to the penalty method [29] to tackle DC constraint C4a and rewrite the problem in (24) as follows

$$\begin{aligned}
 & \underset{\mathbf{x}, \mathbf{W}, \mathbf{B}, \mathbf{U}, \mathbf{V}}{\text{minimize}} \quad \bar{P}(\mathbf{W}, \mathbf{B}) + \frac{1}{\mu} \sum_{m=1}^M \sum_{n=1}^N (b_m[n] - b_m[n]^2) \\
 & \text{s.t.} \quad \text{C1a, C1b, } \overline{\text{C2}}, \text{C3, } \overline{\text{C4}}, \text{C5, C6a, C6b,}
 \end{aligned} \tag{34}$$

Algorithm 3 Suboptimal Resource Allocation Algorithm for Perfect CSI

- 1: Set iteration index $j = 0$ and generate a feasible $\mathbf{B}^{(0)}$. Set convergence tolerance $0 < \Delta_{\text{SCA}} \ll 1$ and penalty factor $0 < \mu \ll 1$
 - 2: **repeat**
 - 3: Set $j = j + 1$
 - 4: Solve (35) for a given $\mathbf{B}^{(j-1)}$ and update $\mathbf{B}^{(j)}$ as the optimal solution of (35)
 - 5: **until** $\frac{\|\mathbf{B}^{(j-1)} - \mathbf{B}^{(j)}\|_F}{\|\mathbf{B}^{(j-1)}\|_F} \leq \Delta_{\text{SCA}}$
-

where $\mu > 0$ is a sufficiently small penalty factor such that problem (24) and problem (34) are equivalent [28]. By applying the SCA technique, we formulate the optimization problem in the $(j + 1)$ -th iteration of the SCA algorithm as

$$\begin{aligned} & \underset{\mathbf{X}, \mathbf{W}, \mathbf{B}, \mathbf{U}, \mathbf{V}}{\text{minimize}} \quad \bar{P}(\mathbf{W}, \mathbf{B}) + \frac{1}{\mu} \sum_{m=1}^M \sum_{n=1}^N (b_m[n] - 2b_m^{(j)}[n]b_m[n] - (b_m^{(j)}[n])^2) \\ & \text{s.t.} \quad \text{C1a, C1b, } \overline{\text{C2}}, \text{C3, } \overline{\text{C4}}, \text{C5, C6a, C6b,} \end{aligned} \quad (35)$$

where $b_m^{(j)}[n]$ is the solution for $b_m[n]$ in the j -th iteration. Note that problem (35) is convex and can be optimally solved by standard convex program solvers such as CVX [25]. The proposed iterative SCA algorithm is summarized in **Algorithm 3**. Some further remarks are given as follows:

- 1) *Initial point*: A matrix, \mathbf{B} , satisfying constraints $\overline{\text{C2}}, \text{C3}, \overline{\text{C4}}$, and C5 is randomly generated.
- 2) *Optimality and convergence*: The solution of problem (35) provides an upper limit for the resource allocation problem in (24). Through solving (35) iteratively, we progressively tighten this upper limit. Note that the proposed suboptimal algorithm converges to a locally optimal solution of (24) [31].
- 3) *Complexity*: In each iteration, we only need to solve one convex programming problem. Thus, **Algorithm 3** exhibits polynomial computational complexity [31]. Specifically, given that the problem in (35) involves K second-order cone (SOC) constraints involving optimization variable $\mathbf{X} \in \mathbb{C}^{N \times K}$ with a cone dimension of $\mathcal{O}(K)$, the computational complexity of each iteration of the proposed SCA-based algorithm is given by $\mathcal{O}\left(\log \frac{1}{\rho}(K^{\frac{7}{2}}N^3 + K^{\frac{7}{2}}N^2 + K^{\frac{7}{2}})\right)$ [30, Theorem 3.11].

IV. ALGORITHM DESIGN FOR IMPERFECT CSI

In this section, we reformulate the resource allocation problem in (19) accounting for imperfect CSI based on the norm-bounded error model in (7). In particular, we aim to minimize the total power consumption at the BS while guaranteeing a worst-case QoS for each user. Since the resulting worst-case QoS constraint consists of infinitely many non-convex inequality constraints introduced by the continuity of the CSI uncertainty set, the worst-case QoS constraint cannot be recast as a series of convex constraints as was done for perfect CSI in Section III-B. Accordingly, we have to suitably modify the BnB-based and SCA-based methods proposed in Section III, respectively, to tackle the new robust resource allocation problem.

A. Problem Reformulation

We formulate a robust resource allocation problem for the considered MA-enabled system exploiting the proposed CSI uncertainty model in (7). Considering the problem in (16), the proposed robust BS beamforming and MA position optimization problem is formulated as follows

$$\begin{aligned} & \underset{\mathbf{W}, \mathbf{B}}{\text{minimize}} \quad \bar{P}(\mathbf{W}, \mathbf{B}) \\ & \text{s.t.} \quad \widehat{\text{C1}} : \min_{\hat{\mathbf{h}}_k \in \Omega_{\hat{\mathbf{h}}_k}} \frac{|\hat{\mathbf{h}}_k^H \mathbf{B} \mathbf{w}_k|^2}{\sum_{k' \in \mathcal{K} \setminus \{k\}} |\hat{\mathbf{h}}_k^H \mathbf{B} \mathbf{w}_{k'}|^2 + \sigma_k^2} \geq \gamma_k, \forall k \in \mathcal{K}, \\ & \quad \quad \quad \bar{\text{C2}}, \text{C3}, \text{C4}, \text{C5}, \end{aligned} \quad (36)$$

where constraint $\widehat{\text{C1}}$ includes infinitely many non-convex inequality constraints due to the continuity of the CSI uncertainty sets, and cannot be reformulated to a convex constraint by Lemma 3. Instead, the numerator of the SINR constraint $\widehat{\text{C1}}$ can be rewritten as $|\hat{\mathbf{h}}_k^H \mathbf{B} \mathbf{w}_k|^2 = \hat{\mathbf{h}}_k^H \mathbf{B} \mathbf{W}_k \mathbf{B}^H \hat{\mathbf{h}}_k$, where $\mathbf{W}_k = \mathbf{w}_k \mathbf{w}_k^H$. Also, the denominator can be rewritten in a similar manner, and we can recast constraint $\widehat{\text{C1}}$ as follows

$$\widehat{\text{C1}} \Leftrightarrow \min_{\hat{\mathbf{h}}_k \in \Omega_{\hat{\mathbf{h}}_k}} \sigma_k^2 \gamma_k + \hat{\mathbf{h}}_k^H \mathbf{B} \left(\gamma_k \sum_{k' \in \mathcal{K} \setminus \{k\}} \mathbf{W}_{k'} - \mathbf{W}_k \right) \mathbf{B}^H \hat{\mathbf{h}}_k \leq 0. \quad (37)$$

By substituting $\hat{\mathbf{h}}_k = \mathbf{G}_k(\bar{\boldsymbol{\psi}}_k + \Delta \boldsymbol{\psi}_k)$ into (37), we can rewrite constraint $\widehat{\text{C1}}$ as follows

$$\begin{aligned} \widehat{\text{C1}} \Leftrightarrow & \bar{\boldsymbol{\psi}}_k^H \mathbf{G}_k \mathbf{B} \widetilde{\mathbf{W}}_k \mathbf{B}^H \mathbf{G}_k \bar{\boldsymbol{\psi}}_k + \Delta \boldsymbol{\psi}^H \mathbf{G}_k^H \mathbf{B} \widetilde{\mathbf{W}}_k \mathbf{B}^H \mathbf{G}_k \Delta \boldsymbol{\psi}_k \\ & + 2\text{Re}\{\bar{\boldsymbol{\psi}}_k^H \mathbf{G}_k^H \mathbf{B} \widetilde{\mathbf{W}}_k \mathbf{B}^H \mathbf{G}_k \Delta \boldsymbol{\psi}_k\} + \sigma_k^2 \gamma_k \leq 0, \forall \|\Delta \boldsymbol{\psi}_k\|_2^2 \leq \epsilon_k^2, \end{aligned} \quad (38)$$

where $\widetilde{\mathbf{W}}_k = \gamma_k \sum_{k' \in \mathcal{K} \setminus \{k\}} \mathbf{W}_{k'} - \mathbf{W}_k$. Here, constraint $\widehat{\text{C1}}$ consists of infinitely many inequality constraints due to the continuity of the CSI uncertainty sets. To facilitate algorithm design, we apply the following lemma to reformulate constraint $\widehat{\text{C1}}$ to an LMI constraint.

Lemma 4. (Generalized S-Procedure [32]): Let $f_i(\mathbf{x})$, $\forall i \in \{0, \dots, I\}$, be a real-valued function of vector $\mathbf{x} \in \mathbb{C}^{N \times 1}$ and be defined as follows,

$$f_i(\mathbf{x}) = \mathbf{x}^H \mathbf{A}_i \mathbf{x} + 2 \text{Re}\{\mathbf{a}_i^H \mathbf{x}\} + a_i, \quad (39)$$

where $\mathbf{A}_i \in \mathbb{S}^N$, $\mathbf{a}_i \in \mathbb{C}^{N \times 1}$, and $a_i \in \mathbb{R}$, $\forall i \in \{0, \dots, I\}$. Then, the implication $f_i(\mathbf{x}) \leq 0$, $\forall i \in \{1, \dots, I\} \Rightarrow f_0(\mathbf{x}) \leq 0$ holds if and only if there exist some real numbers $\lambda_i \geq 0$, $\forall i \in \{1, \dots, I\}$, such that

$$\sum_{i=1}^I \lambda_i \begin{bmatrix} \mathbf{A}_i & \mathbf{a}_i \\ \mathbf{a}_i^H & a_i \end{bmatrix} - \begin{bmatrix} \mathbf{A}_0 & \mathbf{a}_0 \\ \mathbf{a}_0^H & a_0 \end{bmatrix} \geq \mathbf{0}. \quad (40)$$

By leveraging Lemma 4, robust SINR constraint $\widehat{\text{C1}}$ can be rewritten as follows

$$\mathbf{P}_k - \widetilde{\mathbf{G}}_k^H \mathbf{B} \widetilde{\mathbf{W}}_k \mathbf{B}^H \widetilde{\mathbf{G}}_k \geq \mathbf{0}, \forall k, \quad (41)$$

where

$$\mathbf{P}_k = \begin{bmatrix} q_k \mathbf{I}_{L_k} & \mathbf{0} \\ \mathbf{0} & -q_k \epsilon_k^2 - \sigma_k^2 \gamma_k \end{bmatrix}, \quad \widetilde{\mathbf{G}}_k = [\mathbf{G}_k \quad \mathbf{G}_k \bar{\boldsymbol{\psi}}_k], \quad (42)$$

and $q_k \geq 0$ is an auxiliary variable. We note that SINR constraint $\widehat{\text{C1}}$ is non-convex w.r.t. \mathbf{B} and \mathbf{W}_k due to the coupling between \mathbf{B} and \mathbf{W}_k . Next, we define a new optimization variable $\hat{\mathbf{X}}_k = \mathbf{B} \mathbf{W}_k \mathbf{B}^H$ to recast

the constraint in (41) as follows

$$\widehat{\text{C1}} : \mathbf{P}_k - \tilde{\mathbf{G}}_k^H \tilde{\mathbf{X}}_k \tilde{\mathbf{G}}_k \geq \mathbf{0}, \forall k, \quad (43)$$

where $\tilde{\mathbf{X}}_k = \gamma_k \sum_{k' \in \mathcal{K} \setminus \{k\}} \hat{\mathbf{X}}_{k'} - \hat{\mathbf{X}}_k$. Note that constraint $\widehat{\text{C1}}$ is convex w.r.t. variables $\hat{\mathbf{X}}_k, \forall k$. For the sake of notational simplicity, we define $\hat{\mathbf{X}} = [\hat{\mathbf{X}}_1, \dots, \hat{\mathbf{X}}_K]$ to collect all $\hat{\mathbf{X}}_k, \forall k$. Then, (36) can be recast as the following optimization problem:

$$\begin{aligned} & \underset{\mathbf{W}, \mathbf{B}, \hat{\mathbf{X}}}{\text{minimize}} \quad \bar{P}(\mathbf{W}, \mathbf{B}) \\ & \text{s.t.} \quad \widehat{\text{C1}}, \overline{\text{C2}}, \text{C3-C5}, \text{C7} : \hat{\mathbf{X}}_k = \mathbf{B} \mathbf{W}_k \mathbf{B}^H, \forall k \in \mathcal{K}, \end{aligned} \quad (44)$$

Note that C7 is a non-convex constraint due to the coupled variables \mathbf{W}_k and \mathbf{B} . In particular, equality constraint C7 is neither a bilinear nor a biconvex constraint. However, thanks to the binary nature of \mathbf{B} , we are able to convexify constraint C7 by exploiting the following lemma.

Lemma 5. *Equality constraint C7 is equivalent to the following LMI constraints,*

$$\begin{aligned} \text{C7a} : & \begin{bmatrix} \hat{\mathbf{S}}_k & \hat{\mathbf{X}}_k & \mathbf{B} \\ \hat{\mathbf{X}}_k^H & \hat{\mathbf{T}}_k & \mathbf{Y}_k \\ \mathbf{B}^H & \mathbf{Y}_k^H & \mathbf{I}_M \end{bmatrix} \geq \mathbf{0}, \quad \text{C7c:} \begin{bmatrix} \mathbf{U}_k & \mathbf{Y}_k & \mathbf{B} \\ \mathbf{Y}_k^H & \mathbf{V}_k & \mathbf{W}_k \\ \mathbf{B}^H & \mathbf{W}_k^H & \mathbf{I}_M \end{bmatrix} \geq \mathbf{0}, \\ \text{C7b} : & \text{Tr}(\hat{\mathbf{S}}_k) - M \leq 0, \quad \text{C7d:} \text{Tr}(\mathbf{U}_k) - M \leq 0, \end{aligned} \quad (45)$$

where $\hat{\mathbf{S}}_k \in \mathbb{C}^{N \times N}$, $\hat{\mathbf{T}}_k \in \mathbb{C}^{N \times N}$, $\mathbf{Y}_k \in \mathbb{C}^{N \times M}$, $\mathbf{U}_k \in \mathbb{C}^{N \times N}$, and $\mathbf{V}_k \in \mathbb{C}^{M \times M}$ are the auxiliary variables.

Proof. Please refer to Appendix C. □

For convenience, we define $\hat{\mathbf{S}} = [\hat{\mathbf{S}}_1, \dots, \hat{\mathbf{S}}_K]$, $\hat{\mathbf{T}} = [\hat{\mathbf{T}}_1, \dots, \hat{\mathbf{T}}_K]$, $\mathbf{U} = [\mathbf{U}_1, \dots, \mathbf{U}_K]$, $\mathbf{V} = [\mathbf{V}_1, \dots, \mathbf{V}_K]$, $\mathbf{Y} = [\mathbf{Y}_1, \dots, \mathbf{Y}_K]$, $\mathbf{q} = [q_1, \dots, q_K]^T$, and $\hat{\mathbf{W}} = [\mathbf{W}_1, \dots, \mathbf{W}_K]$. Moreover, $\Gamma = \{\mathbf{W}, \mathbf{q}, \hat{\mathbf{X}}, \mathbf{Y}, \hat{\mathbf{S}}, \hat{\mathbf{T}}, \mathbf{V}, \mathbf{U}\}$ collects all optimization variable except \mathbf{B} . Then, the proposed robust resource allocation problem in (44) can be recast as follows

$$\begin{aligned} & \underset{\Gamma, \mathbf{B}, \mathbf{q}}{\text{minimize}} \quad \tilde{P}(\hat{\mathbf{W}}, \mathbf{B}) = \frac{\sum_{m \in \mathcal{M}} \mathbf{b}_m^T \mathbf{e}_m + \sum_{k \in \mathcal{K}} \text{Tr}(\mathbf{W}_k) T_{\text{Data}}}{T_{\text{MA}} + T_{\text{Data}}} \\ & \text{s.t.} \quad \widehat{\text{C1}}, \overline{\text{C2}}, \text{C3}, \text{C4}, \text{C5}, \text{C7a}, \text{C7b}, \text{C7c}, \text{C7d}, \end{aligned} \quad (46)$$

$$\text{C8: rank}(\mathbf{W}_k) = 1, \forall k \in \mathcal{K},$$

$$\text{C9: } \mathbf{W}_k \geq \mathbf{0}, \forall k \in \mathcal{K}.$$

Optimization problem (46) is non-convex due to binary constraint C4 and rank-one constraint C8. In the following subsection, we introduce a series of transformations to convexify non-convex constraints C4 and C8 and extend the proposed BnB-based algorithm for perfect CSI to the case of imperfect CSI.

B. Proposed BnB-based Algorithm

We first initialize the BnB tree $\hat{\mathcal{T}}^{(0)}$ of the proposed BnB-based algorithm for imperfect CSI. Similar to the notation in Section III-C, the initial search tree $\hat{\mathcal{T}}^{(0)}$ contains one root node $\hat{\mathcal{N}}_0 = \{\hat{\mathcal{B}}^{(0)}, \hat{F}_L^{(0)}, \hat{F}_U^{(0)}\}$,

where $\hat{\mathcal{B}}^{(0)}$, $\hat{F}_L^{(0)}$, and $\hat{F}_U^{(0)}$ denote the initial search space and initial lower and upper bounds of the resource allocation problem in (46), respectively. Here, the initial search space $\hat{\mathcal{B}}^{(0)}$ is the product of $M \times N$ binary sets, i.e., $\hat{\mathcal{B}}^{(0)} = \prod_{(m,n) \in \mathcal{L}} \hat{\mathcal{B}}_{m,n}^{(0)}$, where $\hat{\mathcal{B}}_{m,n}^{(0)} \in \{0, 1\}$, $\forall m, n$, denotes the initial feasible set of $b_m[n]$.

We then derive the initial lower and upper bounds for the considered MA-enabled MIMO systems. In particular, to facilitate the derivation of the lower bound, we relax the initial binary search space to convex set $\bar{\mathcal{B}}^{(0)} = \prod_{(m,n) \in \mathcal{L}} \bar{\mathcal{B}}_{m,n}^{(0)}$ with $\bar{\mathcal{B}}_{m,n}^{(0)} = \{b_m[n] \mid 0 \leq b_m[n] \leq 1\}$, $\forall m, n$. Moreover, we tackle rank-one constraint C8 by SDR [33]–[35]. Thus, a lower bound of (46) is obtained by solving the following optimization problem

$$\begin{aligned} & \underset{\Gamma, \mathbf{B}}{\text{minimize}} \quad \tilde{P}(\hat{\mathbf{W}}, \mathbf{B}) \\ & \text{s.t.} \quad \widehat{\text{C1}}, \widehat{\text{C2}}, \text{C3}, \text{C5}, \text{C7a-C7d}, \text{C9}, \overline{\text{C4}} : \mathbf{B} \in \bar{\mathcal{B}}^{(0)}. \end{aligned} \quad (47)$$

The tightness of the relaxation is revealed in the following theorem.

Theorem 1. *If the problem in (47) is feasible, there always exists an optimal beamforming matrix $\mathbf{W}_k^{\text{opt}}$ with $\text{rank}(\mathbf{W}_k^{\text{opt}}) \leq 1, \forall k$.*

Proof. Please refer to Appendix D. □

Note that the problem in (47) is jointly convex w.r.t. Γ and \mathbf{B} . Similar to the notation in Section III-C, let $\Gamma_L^{(0)}$ and $\hat{\mathbf{B}}_L^{(0)}$ denote the optimal solutions of Γ and \mathbf{B} for optimization problem (47), respectively. Then, the initial lower bound $\hat{F}_L^{(0)}$ is given by $\hat{F}_L^{(0)} = \tilde{P}(\hat{\mathbf{W}}_L^{(0)}, \hat{\mathbf{B}}_L^{(0)})$.

On the other hand, we can obtain an upper bound of (46) based on $\hat{\mathbf{B}}_L^{(0)}$. Following a similar procedure as in **Algorithm 1**, we can construct a binary solution $\hat{\mathbf{B}}_U^{(0)} = [\hat{\mathbf{b}}_{U,1}^{(0)}, \dots, \hat{\mathbf{b}}_{U,M}^{(0)}]$ based on $\hat{\mathbf{B}}_L^{(0)}$ by minimizing the Euclidean distance between $\hat{\mathbf{B}}_L^{(0)}$ and $\hat{\mathbf{B}}_U^{(0)}$. Then, an upper bound for (46) is obtained by solving the following optimization problem

$$\begin{aligned} & \underset{\Gamma, \mathbf{B}=\hat{\mathbf{B}}_U^{(0)}}{\text{minimize}} \quad \tilde{P}(\hat{\mathbf{W}}, \mathbf{B}) \\ & \text{s.t.} \quad \widehat{\text{C1}}, \text{C7a}, \text{C7b}, \text{C7c}, \text{C7d}, \text{C9}. \end{aligned} \quad (48)$$

Here, although the rank-one constraint is relaxed, the tightness of the rank-one relaxation is given by the following theorem.

Theorem 2. *If the problem in (48) is feasible for a given \mathbf{B} , there always exists an optimal beamforming matrix $\mathbf{W}_k^{\text{opt}}$ with $\text{rank}(\mathbf{W}_k^{\text{opt}}) \leq 1, \forall k$.*

Proof. The proof follows the same steps as that for Theorem 1 and is omitted here. □

Note that the optimization problem in (48) is convex w.r.t. the variables in Γ . Thus, the optimal solution of (48) can be obtained by CVX. Here, we denote the obtained optimal solution of $\hat{\mathbf{W}}$ as $\hat{\mathbf{W}}_U^{(0)} = [\mathbf{W}_{U,1}^{(0)}, \dots, \mathbf{W}_{U,K}^{(0)}]$ and the initial upper bound $\hat{F}_U^{(0)}$ is given by $\hat{F}_U^{(0)} = \tilde{P}(\hat{\mathbf{W}}_U^{(0)}, \mathbf{B}_f^{(0)})$.

In the t -th iteration of the proposed BnB-based algorithm, we denote $\hat{\mathcal{T}}^{(t-1)}$ as the BnB tree obtained in the last iteration. Similar to the notations in Section III-C, we let sets $\hat{\mathcal{I}}^{(t-1)}$ and $\hat{\mathcal{E}}^{(t-1)}$ denote the collections of the internal and external nodes of the BnB tree $\hat{\mathcal{T}}^{(t-1)}$. Then, we select the node $\hat{\mathcal{N}}_{\hat{i}_t} = \{\hat{\mathcal{B}}^{(\hat{i}_t)}, \hat{F}_L^{(\hat{i}_t)}, \hat{F}_U^{(\hat{i}_t)}\}$, $\hat{\mathcal{N}}_{\hat{i}_t} \in \hat{\mathcal{E}}^{(t-1)}$, from the external nodes of BnB tree $\hat{\mathcal{T}}^{(t-1)}$ with the smallest lower bound $\hat{F}_L^{(\hat{i}_t)}$, where \hat{i}_t denotes the index of the selected node from $\hat{\mathcal{T}}^{(t-1)}$ at the t -th iteration. Moreover, $\hat{\mathcal{B}}^{(\hat{i}_t)} = \prod_{(m,n) \in \mathcal{L}} \hat{\mathcal{B}}_{m,n}^{(\hat{i}_t)}$ denotes the binary search space for matrix \mathbf{B} corresponding to the selected node $\hat{\mathcal{N}}_{\hat{i}_t}$ and $\hat{\mathcal{B}}_{m,n}^{(\hat{i}_t)}$ is the search space for binary variable $b_m[n]$. Here, $\hat{\mathcal{B}}^{(\hat{i}_t)}$ contains the binary sets corresponding to both the determined and undetermined binary variables. To simplify notation, we define $\hat{\mathcal{U}}^{(\hat{i}_t)}$ and $\hat{\mathcal{D}}^{(\hat{i}_t)}$ as the collections of the indices of undetermined and determined binary variables in $\hat{\mathcal{B}}^{(\hat{i}_t)}$, respectively.

Then, following a similar procedure as in Section III-C, we partition the selected node $\hat{\mathcal{N}}_{\hat{i}_t}$ into two child nodes based on the Euclidean distance between the optimal solution for the lower bound $\hat{\mathbf{B}}_L^{(\hat{i}_t)}$ and its binary version $\hat{\mathbf{B}}_U^{(\hat{i}_t)}$. Specifically, we first obtain the index $(\hat{m}^{(t)}, \hat{n}^{(t)})$ based on

$$(\hat{m}^{(t)}, \hat{n}^{(t)}) = \arg \max_{m,n} |\hat{b}_{L,m}^{(\hat{i}_t)}[n] - \hat{b}_{U,m}^{(\hat{i}_t)}[n]|, \quad (49)$$

where $\hat{b}_{L,m}^{(\hat{i}_t)}[n]$ and $\hat{b}_{U,m}^{(\hat{i}_t)}[n]$ represent the n -th element in the m -th column of $\hat{\mathbf{B}}_L^{(\hat{i}_t)}$ and $\hat{\mathbf{B}}_U^{(\hat{i}_t)}$, respectively. Next, the feasible set for \mathbf{B} of the selected node, i.e., $\hat{\mathcal{B}}^{(\hat{i}_t)}$ is divided into two new subsets corresponding to $b_{\hat{m}^{(t)}}[\hat{n}^{(t)}] = 0$ and $b_{\hat{m}^{(t)}}[\hat{n}^{(t)}] = 1$, respectively. Then, the resource allocation problems $\hat{\mathcal{P}}_i, i \in \{0, 1\}$, for the two child nodes are given by

$$\begin{aligned} \hat{\mathcal{P}}_i : & \underset{\mathbf{r}, \mathbf{B}}{\text{minimize}} \quad \tilde{P}(\hat{\mathbf{W}}, \mathbf{B}) \\ \text{s.t.} \quad & \widehat{\mathbf{C1}}, \widehat{\mathbf{C2}}, \mathbf{C3}, \mathbf{C5}, \mathbf{C7a}, \mathbf{C7b}, \mathbf{C7c}, \mathbf{C7d}, \mathbf{C9}, \\ & \widehat{\mathbf{C4a}} : b_m[n] \in \hat{\mathcal{B}}_{m,n}^{(\hat{i}_t)}, \widehat{\mathbf{C4b}} : b_{\hat{m}^{(t)}}[\hat{n}^{(t)}] = i. \end{aligned} \quad (50)$$

Note that constraint $\widehat{\mathbf{C4a}}$ is non-convex due to the discreteness of search space $\hat{\mathcal{B}}^{(\hat{i}_t)}$. Similar to the procedure for deriving the initial lower bound, we relax the undetermined binary variables $b_m[n], \forall (m, n) \in \hat{\mathcal{U}}^{(\hat{i}_t)} \setminus (\hat{m}^{(t)}, \hat{n}^{(t)})$ to continuous bounded variables, i.e., $0 \leq b_m[n] \leq 1$. Then, a lower bound of (50) is obtained by solving the following relaxed optimization problem $\hat{\tilde{\mathcal{P}}}_i, i \in \{0, 1\}$

$$\begin{aligned} \hat{\tilde{\mathcal{P}}}_i : & \underset{\mathbf{r}, \mathbf{B}}{\text{minimize}} \quad \tilde{P}(\hat{\mathbf{W}}, \mathbf{B}) \\ \text{s.t.} \quad & \widehat{\mathbf{C1}}, \widehat{\mathbf{C2}}, \mathbf{C3}, \widehat{\mathbf{C4b}}, \mathbf{C5}, \mathbf{C7a}, \mathbf{C7b}, \mathbf{C7c}, \mathbf{C7d}, \mathbf{C9}, \\ & \widehat{\mathbf{C4c}} : b_m[n] \in \hat{\mathcal{B}}_{m,n}^{(\hat{i}_t)}, \forall (m, n) \in \hat{\mathcal{D}}^{(\hat{i}_t)} \\ & \widehat{\mathbf{C4d}} : 0 \leq b_m[n] \leq 1, \forall (m, n) \in \hat{\mathcal{U}}^{(\hat{i}_t)} \setminus (\hat{m}^{(t)}, \hat{n}^{(t)}), \end{aligned} \quad (51)$$

which is a convex problem, and the optimal solution can be attained by standard convex solvers such as CVX. Here, the optimal \mathbf{B} and $\hat{\mathbf{W}}$ for $\hat{\tilde{\mathcal{P}}}_0$ and $\hat{\tilde{\mathcal{P}}}_1$ are denoted as $(\hat{\mathbf{B}}_{L,0}^{(t)}, \hat{\mathbf{W}}_{L,0}^{(t)})$ and $(\hat{\mathbf{B}}_{L,1}^{(t)}, \hat{\mathbf{W}}_{L,1}^{(t)})$, respectively. Therefore, lower bounds corresponding to problem $\hat{\mathcal{P}}_0$ and $\hat{\mathcal{P}}_1$ are given by $\tilde{P}(\hat{\mathbf{W}}_{L,0}^{(t)}, \hat{\mathbf{B}}_{L,0}^{(t)})$

and $\tilde{P}(\hat{\mathbf{W}}_{L,1}^{(t)}, \hat{\mathbf{B}}_{L,1}^{(t)})$, respectively.

Next, following a similar procedure as in Section III-C, we generate a feasible binary matrix $\hat{\mathbf{B}}_{U,i}^{(t)}$ based on $\hat{\mathbf{B}}_{L,i}^{(t)}$ by employing **Algorithm 1**, where $i \in \{0, 1\}$. Then, an upper bound corresponding to the new node with $b_{\hat{n}^{(t)}}[\hat{n}^{(t)}] = i$ can be obtained by solving the optimization problem in (48) with $\mathbf{B} = \hat{\mathbf{B}}_{U,i}^{(t)}$, $i \in \{0, 1\}$. Note that the optimization problem in (48) is convex with given $\mathbf{B} = \hat{\mathbf{B}}_{U,i}^{(t)}$, $i \in \{0, 1\}$, and can be optimally solved. We let $\hat{\mathbf{W}}_{U,i}^{(t)}$ denote the corresponding optimal solution of $\hat{\mathbf{W}}$ obtained by solving (48) with $\mathbf{B} = \hat{\mathbf{B}}_{U,i}^{(t)}$, $i \in \{0, 1\}$. A lower bound of problem $\hat{\mathcal{P}}_i$ in (50) is given by $\tilde{P}(\hat{\mathbf{W}}_{U,i}^{(t)}, \hat{\mathbf{B}}_{U,i}^{(t)})$, where $i \in \{0, 1\}$.

The resulting BnB-based algorithm has a similar form as **Algorithm 2**. Specifically, in each iteration, we insert two nodes in the BnB tree by solving four SDP problems. Each SDP problem involves K LMI constraints of size $(L_k + 1) \times (L_k + 1)$ due to $\widehat{\mathbf{C}}1$, K LMI constraints of size $(2N + M) \times (2N + M)$ due to C7a, K LMI constraints of size $(2M + N) \times (2M + N)$ due to C7c, and K LMI constraints of size $M \times M$ due to C9. Therefore, the computational complexity in each iteration for solving one SDP problem is given by $\mathcal{O}(\log \frac{1}{\rho}(K((L_{\max} + 1)^3 + (2N + M)^3 + (2M + N)^3 + M^3) + K^2((L_{\max} + 1)^2 + (2N + M)^2 + (2M + N)^2 + M^2) + K^3))$ [30, Theorem 3.12], where $L_{\max} = \max_{k \in \mathcal{K}}(L_k)$. Moreover, the BnB tree update, the convergence, and the optimality analysis are identical to those for **Algorithm 2** in Section III-C, and are not described here in detail due to the page limitation.

C. Proposed SCA-based Algorithm

Following similar steps as for derivation of (27) and (29), applying SDP relaxation to address rank-one constraint C8 and exploiting SCA, we obtain the following optimization problem to be solved in the $(j+1)$ -th iteration of the SCA algorithm

$$\begin{aligned} & \underset{\mathbf{r}, \mathbf{B}}{\text{minimize}} \quad \tilde{P}(\hat{\mathbf{W}}, \mathbf{B}) + \frac{1}{\mu} \sum_{m=1}^M \sum_{n=1}^N (b_m[n] - 2b_m^{(j)}[n]b_m[n] - (b_m^{(j)}[n])^2) \\ & \text{s.t.} \quad \widehat{\mathbf{C}}1, \overline{\mathbf{C}}2, \mathbf{C}3, \overline{\mathbf{C}}4, \mathbf{C}5, \mathbf{C}7a, \mathbf{C}7b, \mathbf{C}7c, \mathbf{C}7d, \mathbf{C}9, \end{aligned} \quad (52)$$

where $b_m^{(j)}[n]$ denotes the solution of $b_m[n]$ obtained in the j -th iteration. The above problem is convex and can be optimally solved by CVX. The proof of the tightness of the SDP relaxation is similar to the proof of Theorem 1. The proposed SCA-based algorithm can be summarized in a similar manner as in **Algorithm 3**. In particular, optimization problem (34) is replaced by (52). Moreover, the optimization problem in (52) is similar to problem $\hat{\mathcal{P}}_i$, $i \in \{0, 1\}$, with a slight difference in the objective function. Therefore, the computational complexity in each iteration for solving one SDP problem is given by $\mathcal{O}(\log \frac{1}{\rho}(K((L_{\max} + 1)^3 + (2N + M)^3 + (2M + N)^3 + M^3) + K^2((L_{\max} + 1)^2 + (2N + M)^2 + (2M + N)^2 + M^2) + K^3))$ [30, Theorem 3.12]. The initial point and convergence analysis are identical to those for the SCA-based

algorithm in Section III-D, and thus are omitted here due to the page limitation.

V. NUMERICAL RESULTS

A. Simulation Setting

In this paper, we consider an MA-enabled multi-user MISO system, where the BS is equipped with $M = 4$ MA elements to serve $K = 4$ single-antenna users. The carrier frequency is set to 5 GHz, i.e., the wavelength is $\lambda = 60$ mm. The transmit area is a square area of size $l\lambda \times l\lambda$, where $l = 2$ denotes the normalized transmit area size at the BS. Due to the properties of MA drivers [13], [14], the transmit area is quantized into discrete positions with equal distance d as shown in Fig. 1. The minimum distance D_{\min} is set to 15 mm. The user distances to the BS are uniformly distributed between 20 m to 80 m. The noise variance of each user is set to -80 dBm, $\forall k \in \mathcal{K}$. The channel coefficient $h_k(\mathbf{p}_n)$ between an MA element at position \mathbf{p}_n and the k -th user is modeled by the field response channel model detailed in Section II-B. The elevation and azimuth AoDs, θ_{k,l_k} and ϕ_{k,l_k} , of the l_k -th channel path for the k -th user follows probability density function $f_{\text{AoD}}(\theta_{k,l_k}, \phi_{k,l_k}) = \frac{\cos \theta_{k,l_k}}{2\pi}$, $\theta_{k,l_k} \in [-\pi/2, \pi/2]$, $\phi_{k,l_k} \in [-\pi/2, \pi/2]$. In this work, the initial positions of the MA elements are randomly generated in the transmit area. Moreover, the power consumption of one MA driver, P_{MA} , is set as 8 W^3 , and the time duration of the first and second subframes are $T_{\text{MA}} = 30$ ms and $T_{\text{Data}} = 270$ ms, respectively. In addition, high-speed stepper motors combined with linear actuators are adopted as MA drivers in this work [37], and the angular velocity and step angle of the stepper motors are set to $\omega = 60\pi \text{ rad/s} = 720 \text{ step/s}$ and $\omega_d = \pi/12 \text{ rad}$ [36], respectively. A lead screw with an outer diameter of $D = 10$ mm is adopted as the linear actuator of the MA drivers. Therefore, the maximum speed and step size of MA motion are given by $v_{v,\text{MA}} = v_{h,\text{MA}} = \omega D = 0.94 \text{ mm/ms}$ and $\omega_d D \approx 2 \text{ mm}$, respectively [37]. Thus, the maximal moving distance of MA is given by $D_{v,\text{max}} = D_{h,\text{max}} = v_{\text{MA}} T_{\text{MA}} \approx 28 \text{ mm}$. Without loss of generality, we assume all users impose the same SINR requirement, i.e., $\gamma_k = \gamma$, $\forall k$, and define the maximum normalized estimation error of the path response vector as $\kappa_k = \epsilon_k / \|\bar{\psi}_k\|_F = \kappa$, $\forall k$. The number of channel realizations considered for the presented simulation results is 200.

We consider four baseline schemes for comparison. For baseline scheme 1, the MA elements are fixed at M positions that satisfy the minimum distance constraint and are chosen randomly from \mathcal{P} , i.e., binary matrix \mathbf{B} is randomly chosen but satisfies constraints C2, C3, C4, and C5. The beamforming vectors \mathbf{w}_k are obtained by solving the beamforming problem in (24) and (46) for the randomly chosen binary matrix \mathbf{B} for perfect and imperfect CSI, respectively. For baseline scheme 2, we adopt the AS technique in [38], where the BS is equipped with a $2 \times M$ uniform planar array (UPA) with fixed-position antennas spaced by $\lambda/2 = 30$ mm such that the channels corresponding to different antennas are statistically independent. We

³Here, we adopt a typical power consumption value for commercial stepper motors in [36].

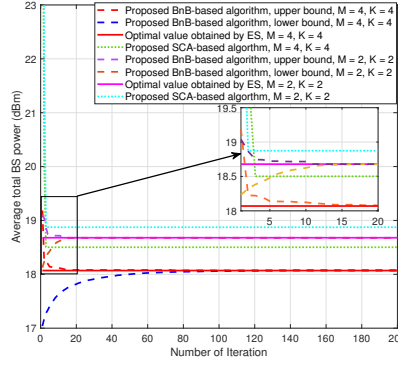


Fig. 4. Convergence behavior of the proposed algorithms for different values of M and K and perfect CSI. The system parameters are set as $\gamma = 5$ dB, and $d = 10$ mm.

solve the beamforming problem in (24) and (46) for all possible subsets of M antenna elements and select the optimal subset that minimizes the BS transmit power, respectively. Note that the antenna spacing cannot be adjusted in baseline scheme 2. As baseline scheme 3, we adopt a suboptimal iterative algorithm based on AO. Specifically, in each iteration, beamforming matrix \mathbf{W} is optimized by solving the problems in (24) and (46) with the fixed binary decision matrix \mathbf{B} obtained in the last iteration for perfect and imperfect CSI, respectively. Afterwards, \mathbf{B} is updated by solving the problems in (24) and (46) by relaxing binary constraint C4 for the fixed \mathbf{W} obtained in the current iteration. After convergence, the obtained continuous binary matrix is quantized to the feasible binary selection matrix \mathbf{B}_{AO} , and the beamforming matrix is designed by solving the problems in (24) and (46) with \mathbf{B}_{AO} . For baseline scheme 4, we jointly design binary decision matrix \mathbf{B} and beamforming matrix \mathbf{W} without taking the power consumption of the MA drivers into account. In particular, we optimally solve the resource allocation problem in (16) and (36) with a modified objective function, i.e., $P = \sum_{k \in \mathcal{K}} \|\mathbf{w}_k\|_2^2$, using the proposed BnB-based method for perfect and imperfect CSI, respectively. Baseline scheme 4 is used to investigate the impact of accounting for the power consumption of the MA drivers on performance.

B. Numerical Results for Perfect CSI

1) *Convergence of the proposed algorithms:* Fig. 4 illustrates the convergence of the proposed BnB-based and SCA-based algorithms for different numbers of MA elements M and users K assuming perfect CSI at the BS. Furthermore, we adopt an exhaustive search (ES) approach, serving as a benchmark, to verify the global optimality of the proposed BnB-based method. Specifically, the ES method solves the problem in (24) for all $\binom{N}{M}$ possible position combinations of M MA elements to attain the global optimum. Due to the high complexity of the ES method, we investigate its performance for a system with a relatively large step size $d = 10$ mm. As can be seen in Fig. 4, the proposed BnB-based method converges to the optimal solution obtained with the ES methods for both considered system settings, which validates the global optimality of the proposed BnB-based method. Moreover, for the system with 4 MA elements, the

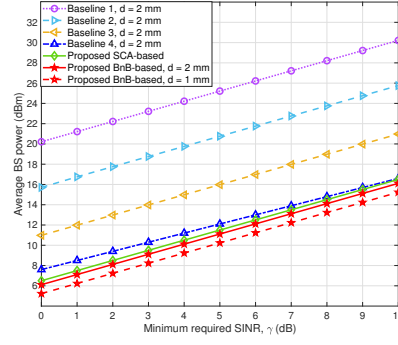


Fig. 5. Average BS power consumption versus the minimum required SINR of the users for perfect CSI. The parameters are set as $M = 4$, $K = 4$, and $l = 2$.

proposed BnB-based algorithm requires only an average of 70 iterations to converge, which is significantly faster than the ES method that requires solving (24) $\binom{N}{M} = \binom{13^2}{4}$ times. On the other hand, the proposed SCA-based algorithm converges to a locally optimal value within 10 iterations, revealing an excellent trade-off between computational complexity and performance.

2) *Average BS power versus minimum required SINR*: Fig. 5 shows the average BS power consumption versus the minimum required SINR γ for perfect CSI. As can be observed, as the minimum required SINR increases, the BS must consume more power to satisfy the more stringent QoS requirements of the users. Moreover, both proposed schemes outperform all four baseline schemes for the entire range of γ . In particular, since for baseline schemes 1 and 2, the BS is equipped with an antenna array with fixed antenna positions, the spatial correlation of the transmit antenna array cannot be shaped in an optimal manner. Moreover, for baseline scheme 3, the adopted AO algorithm tends to search only a subset of the feasible region close to the initial point and is likely to get stuck in a stationary point. Thus, the proposed BnB-based scheme achieves a considerable gain (4 dB) compared to the AO-based scheme. On the other hand, baseline scheme 4 does not account for the power consumption of the MA drivers, resulting in a 1–2 dB performance gap compared to the optimal BnB-based scheme. In particular, the gap between baseline scheme 4 and the BnB-based scheme is reduced as the minimum required SINR increases. This is attributed to the fact that as the minimum required SINR increases, the transmit power consumption becomes more dominant in the overall power consumption and eventually outweighs the impact of the power consumed by the antenna movement. Therefore, baseline scheme 4 yields a solution closer to the global optimum one for very high required SINRs. Furthermore, the proposed SCA-based scheme achieves a performance close to that of the optimal BnB-based scheme. Moreover, it is observed that reducing the step size of the MA drivers from 2 mm to 1 mm leads to a 1.5 dB performance improvement, highlighting the trade-off between BS power consumption and MA control precision in MA-enabled systems.

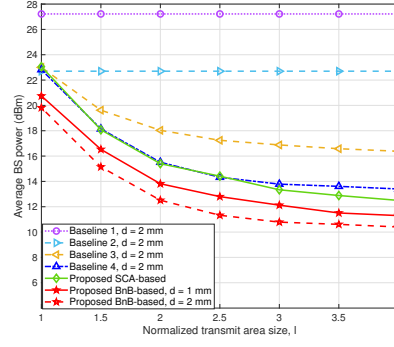


Fig. 6. Average BS power consumption versus the normalized transmit area size of the MA-enabled system for perfect CSI. The parameters are set as $M = 4$, $N = 4$, and $\gamma = 7$ dB.

3) *Average BS power versus transmit area size:* Fig. 6 depicts the average BS power consumption for different normalized transmit area sizes for perfect CSI. It is observed that the BS power consumption for baseline schemes 3 and 4 and the proposed schemes decreases as the normalized transmit area size increases. This can be attributed to the fact that a larger transmit area provides more flexibility for positioning the MA elements to adaptively shape the desired spatial correlation based on the actual needs, leading to a performance gain. On the other hand, baseline schemes 1 and 2, with their fixed antenna positions, cannot benefit from a larger transmit area, indicating that baseline schemes 1 and 2 cannot fully utilize the spatial DoFs provided by larger transmit areas. Moreover, as can be observed, both the proposed SCA-based and BnB-based schemes outperform all four baseline schemes. In particular, for larger transmit areas, the gap between baseline scheme 4 and the proposed BnB-based optimal design is enlarged to 1.5 dB. In particular, increasing the transmit area size leads to a higher power consumption for MA motion. Thus, the impact of the MA motion power on the total power consumption grows and the performance gain of the proposed BnB-based scheme compared to baseline scheme 4 increases. This highlights the importance of balancing the radiated power and the power consumed for MA movement in MA-enabled systems with large transmit areas. Furthermore, the performance of the proposed schemes saturates when the normalized transmit area size reaches 3 due to the speed limitation of the MA drivers, which limits the adaptability within one frame.

4) *Average BS power versus the number of MA elements:* We investigate the BS power consumption as a function of the number of MA elements M in Fig. 7. As can be observed, the system performance of all schemes improves significantly by adding more antenna elements. This can be attributed to the extra diversity gain provided by the additional antenna elements. Moreover, the performance gap between the proposed schemes and baseline schemes 1, 2, and 3 is enlarged significantly as the number of antenna elements decreases. Specifically, in a high-load system with $K = M$, baseline schemes 1 and 2 struggle to efficiently suppress the inter-user interference due to the strong correlation of the users' channel vectors.

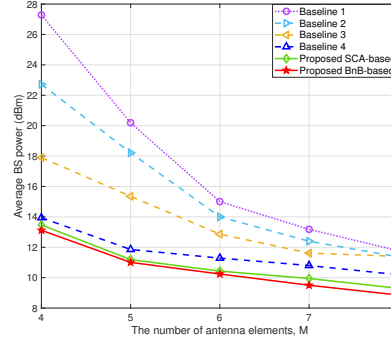


Fig. 7. Average BS power consumption versus the number of MA elements of the MA-enabled system for perfect CSI. The parameters are set as $K = 4$, $l = 2$, $d = 2$ mm, and $\gamma = 7$ dB.

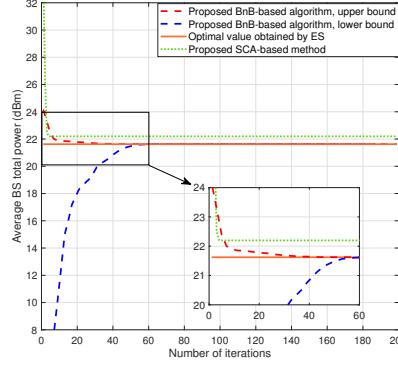


Fig. 8. Convergence behavior of the proposed algorithms for imperfect CSI. The system parameters are set as $M = 2$, $K = 2$, $\gamma = 5$ dB, $d = 10$ mm, and $\kappa = 0.1$.

On the other hand, as MAs can reshape the channel correlation, both the proposed SCA- and BnB-based schemes can reduce inter-user interference by optimizing the MA positions. Moreover, compared with AO-based baseline scheme 3, the proposed SCA- and BnB-based methods achieve a 5 dB performance gain in a high-load system with $K = M$, which highlights the importance of an efficient optimization of the MA position and BS beamforming in such a scenario.

C. Numerical Results for Imperfect CSI

1) *Convergence of the proposed algorithms:* Fig. 8 illustrates the convergence behavior of the proposed schemes for imperfect CSI. Here, to verify optimality, we adopt again an ES method as a benchmark, which solves the optimization problem in (46) for all $\binom{N}{M}$ possible MA position configurations to attain the global optimum of (36). Due to the high computational complexity of the ES algorithm, we only investigate its performance for a MIMO system with $M = 2$ and $K = 2$. As can be observed, the proposed BnB-based scheme converges to a solution identical to the global optimum obtained by the ES method, which confirms the optimality of the proposed BnB-based method. Moreover, the proposed BnB-based method converges to the global optimum in 60 iterations, which is much faster than the brute-force ES method. On the other hand, the BnB-based algorithm proposed for imperfect CSI requires more iterations to converge compared

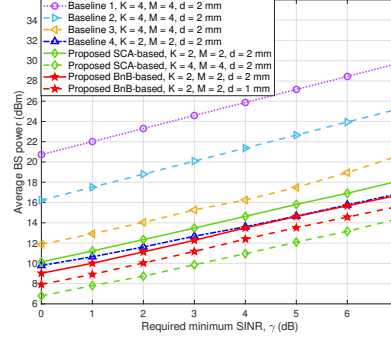


Fig. 9. Average BS power consumption versus the minimum required SINR of the users for imperfect CSI. The system parameters are set as $l = 2$ and $\kappa = 0.1$.

to the algorithm for perfect CSI, e.g., Fig. 4. In fact, for imperfect CSI, we had to introduce a series of auxiliary variables and SDP constraints to tackle the robust constraint and the intricate coupling between \mathbf{W}_k and \mathbf{B} , which inevitably reduces the speed of convergence. Furthermore, the proposed SCA-based scheme achieves close-to-optimal performance within only 10 iterations, revealing its computational efficiency for robust system design.

2) *Average BS power versus minimum required SINR*: Fig. 9 shows the average BS power consumption versus the minimum required SINR for imperfect CSI. Due to the exponential growth in the computational complexity of the proposed BnB-based algorithm w.r.t. the number of MA elements M , we simulate the performance of the proposed BnB-based algorithm and baseline scheme 4 for a small value of M , i.e., $M = 2$. As can be observed, the proposed SCA- and BnB-based algorithms reduce the BS power consumption significantly compared to baseline schemes 1, 2, and 3. In particular, for the system with $M = 4$ MA elements and $K = 4$ users, the proposed SCA-based method achieves a gain of 4-5.5 dB compared to AO-based baseline scheme 3. The results obtained by the AO-based scheme have to be quantized to a feasible binary selection matrix after convergence. However, coarse quantization leads to mismatches in robust beamforming and interference suppression, causing significant performance degradation. This mismatch becomes more pronounced as the QoS requirements become more severe, as can be observed in Fig. 9. On the other hand, the proposed low-complexity SCA-based scheme achieves a performance close to that of the optimal BnB-based scheme for a system with $M = 2$ MA elements and $K = 2$ users, thereby highlighting the excellent performance-complexity tradeoff of the proposed SCA-based method.

3) *Average BS power versus the transmit area size*: In Fig. 10, we investigate the average BS power consumption as a function of the normalized transmit area size. Similar to Fig. 6, as the normalized transmit area size increases, the BS power consumed for the proposed schemes and baseline scheme 3 decreases, which can be attributed to the extra DoFs introduced by a larger transmit area. Moreover, the performance gap between the proposed SCA- and BnB-based schemes widens as the transmit area size increases. In

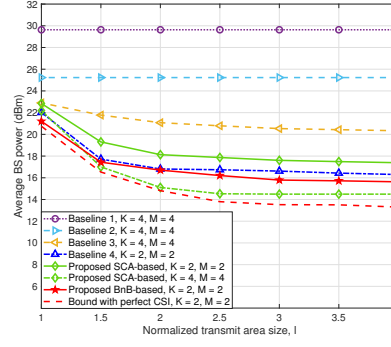


Fig. 10. Average BS power consumption versus the normalized transmit area size of the MA-enabled system for imperfect CSI. The system parameters are set as $\gamma = 7$ dB, $d = 2$ mm, and $\kappa = 0.1$.

fact, increasing the size of the transmit area introduces more binary decision variables that are required to be relaxed in the SCA-based method, which makes the SCA-based method more likely to converge to a local optimum. Thus, the proposed SCA-based scheme becomes more prone to converging to a local optimum with suboptimal performance. Moreover, as can be observed in Fig. 10 the gap between the optimal performances for perfect and imperfect CSI also increases as the size of the transmit region expands. In particular, a larger transmit area size increases the size of the effective channel vectors $\hat{\mathbf{h}}_k$, leading to an enlarged feasible region for the CSI uncertainty. Therefore, the BS has to allocate more transmit power to compensate the larger CSI estimation errors as the size of the transmit region increases.

VI. CONCLUSION

In this paper, we investigated for the first time the globally optimal resource allocation design for a multi-user MA-enabled downlink MISO communication system for both perfect and imperfect CSI. Due to practical hardware limitations, we modeled the motion and energy consumption of the MA in a discrete manner. Then, for both perfect and imperfect CSI, we formulated resource allocation problems for minimization of the total BS power consumption, comprising the radiated and MA motion powers, while guaranteeing a minimum required SINR for each user. To tackle the coupling between the MA positions and the beamforming vectors, we leveraged several transformations and auxiliary variables to recast the formulated optimization problems as tractable MINLP problems. To fully reveal the potential of MA, we proposed BnB-based algorithms for the jointly optimal design of the MA positions and BS beamforming for perfect and imperfect CSI, respectively. Moreover, to reduce computational complexity, we leveraged the SCA technique to obtain locally optimal solutions with polynomial time complexity. Our simulation results verified the global optimality of the proposed BnB-based algorithms and demonstrated the effectiveness in SCA-based algorithms. Moreover, we highlighted the robustness of the proposed BnB-based and SCA-based algorithms to imperfect CSI, ensuring high performance even in the presence of uncertain channel conditions. Furthermore, for both perfect and imperfect CSI, the proposed SCA-based algorithms attained

high performance, offering significant advantages for real-time implementation. Additionally, we showed that the proposed MA-enabled systems reduce the BS power consumption significantly compared to conventional fixed-antenna systems, especially in high-load scenarios with a limited number of antenna elements.

APPENDIX A

PROOF OF LEMMA 1

Based on [39, Lemma 1], equality constraint C6 is equivalent to LMI constraint C6a and inequality constraint:

$$\overline{\text{C6b}}: \text{Tr}(\mathbf{U} - \mathbf{B}\mathbf{B}^H) \leq 0. \quad (53)$$

The left-hand side of (53) can be rewritten as

$$\text{Tr}(\mathbf{U} - \mathbf{B}\mathbf{B}^H) \stackrel{(a)}{=} \text{Tr}(\mathbf{U}) - \sum_{m \in \mathcal{M}} \text{Tr}(\mathbf{b}_m \mathbf{b}_m^H) \stackrel{(b)}{=} \text{Tr}(\mathbf{U}) - M, \quad (54)$$

where equalities (a) and (b) hold due to the additivity of the matrix trace and the definition of binary decision vector $\mathbf{b}_m, \forall m$, respectively. Thus, inequalities C6b and $\overline{\text{C6b}}$ are equivalent, which completes our proof.

APPENDIX B

PROOF OF LEMMA 2

First, we can reformulate constraint C2 as follows,

$$\text{C2} \Leftrightarrow \mathbf{b}_m^T (-\mathbf{D}) \mathbf{b}_{m'} + D_{\min} \leq 0, \quad m \neq m', \quad \forall m, m' \in \mathcal{M}. \quad (55)$$

Next, by defining binary vector $\bar{\mathbf{b}} = [\mathbf{b}_1^T, \dots, \mathbf{b}_M^T]^T$, we can obtain the following equality

$$\mathbf{b}_m = \hat{\mathbf{I}}_m \bar{\mathbf{b}}, \quad (56)$$

where $\hat{\mathbf{I}}_m = [\mathbf{0}_{N \times (m-1)N}, \mathbf{I}_N, \mathbf{0}_{N \times (M-m)N}]$. Then, we can rewrite C2 in (55) equivalently as follows

$$\begin{aligned} \text{C2} &\Leftrightarrow \bar{\mathbf{b}}^T \hat{\mathbf{I}}_m^T (-\mathbf{D}) \hat{\mathbf{I}}_{m'} \bar{\mathbf{b}} + D_{\min} \leq 0 \\ &\Leftrightarrow \bar{\mathbf{b}}^T \left(\frac{-\mathbf{D}_{m,m'} - \mathbf{D}_{m,m'}^T}{2} \right) \bar{\mathbf{b}} + D_{\min} \leq 0, \end{aligned} \quad (57)$$

where $\mathbf{D}_{m,m'} = \hat{\mathbf{I}}_m^T \mathbf{D} \hat{\mathbf{I}}_{m'}$. Moreover, based on the definition of matrix \mathbf{B} , the following equality can be obtained.

$$\bar{\mathbf{b}}^T \bar{\mathbf{b}} = \text{Tr}(\mathbf{B}^T \mathbf{B}) = M. \quad (58)$$

Then, by adding $\eta \bar{\mathbf{b}}^T \bar{\mathbf{b}}$ to both sides of (57), C2 can be rewritten as

$$\begin{aligned} &\bar{\mathbf{b}}^T \left(\frac{-\mathbf{D}_{m,m'} - \mathbf{D}_{m,m'}^T}{2} \right) \bar{\mathbf{b}} + D_{\min} + \eta \bar{\mathbf{b}}^T \bar{\mathbf{b}} \leq \eta \bar{\mathbf{b}}^T \bar{\mathbf{b}} \\ &\bar{\mathbf{b}}^T \left(\frac{-\mathbf{D}_{m,m'} - \mathbf{D}_{m,m'}^T}{2} + \eta \mathbf{I}_{MN} \right) \bar{\mathbf{b}} + D_{\min} \leq \eta M \\ &\bar{\mathbf{b}}^T \left(\frac{-\mathbf{D}_{m,m'} - \mathbf{D}_{m,m'}^T}{2} + \eta \mathbf{I}_{MN} \right) \bar{\mathbf{b}} - \eta M + D_{\min} \leq 0, \end{aligned} \quad (59)$$

which completes the proof.

APPENDIX C

PROOF OF LEMMA 5

We first define an auxiliary variable \mathbf{Y}_k as $\mathbf{Y}_k = \mathbf{B}\mathbf{W}_k^H$. Then, constraint C7 can be recast into the following bilinear constraints

$$\text{C7} \Leftrightarrow \hat{\mathbf{X}}_k = \mathbf{B}\mathbf{Y}_k^H, \quad \mathbf{Y}_k = \mathbf{B}\mathbf{W}_k^H. \quad (60)$$

Based on Lemma 1, $\hat{\mathbf{X}}_k = \mathbf{B}\mathbf{Y}_k^H$ can be rewritten as constraint C7a and an inequality constraint:

$$\text{Tr}(\hat{\mathbf{S}}_k - \mathbf{B}\mathbf{B}^H) \leq 0. \quad (61)$$

Because of the binary nature of \mathbf{B} , we can rewrite (61) as the following linear inequality constraint

$$\begin{aligned} \text{Tr}(\hat{\mathbf{S}}_k - \mathbf{B}\mathbf{B}^H) &\Leftrightarrow \text{Tr}(\hat{\mathbf{S}}_k) - \text{Tr}(\mathbf{B}\mathbf{B}^H) \\ &\Leftrightarrow \text{C7b} : \text{Tr}(\hat{\mathbf{S}}_k) - M \leq 0. \end{aligned} \quad (62)$$

Similar to the above approach, we can recast constraint $\mathbf{Y}_k = \mathbf{W}_k\mathbf{B}^H$ as constraints C7c and C7d, which completes the proof.

APPENDIX D

PROOF OF THEOREM 1

The problem in (47) is convex w.r.t. $\hat{\mathbf{W}}, \hat{\mathbf{X}}, \mathbf{B}, \hat{\mathbf{S}}, \hat{\mathbf{T}}, \mathbf{U}, \mathbf{V}, \mathbf{Y}$, and \mathbf{q} and Slater's condition is satisfied [32], [33]. Thus, strong duality holds and the optimal Lagrangian multipliers for constraints $\widehat{\text{C1}}, \text{C7a}, \text{C7c}, \text{C9}$ are given by $\mathbf{A}_k, \hat{\mathbf{Q}}_k, \hat{\mathbf{\Xi}}_k$, and \mathbf{Z}_k , respectively. Here, $\hat{\mathbf{Q}}_k$ and $\hat{\mathbf{\Xi}}_k$ are decomposed as follows

$$\hat{\mathbf{Q}}_k = \begin{bmatrix} \hat{\mathbf{Q}}_{k,11} & \hat{\mathbf{Q}}_{k,21}^H & \hat{\mathbf{Q}}_{k,31}^H \\ \hat{\mathbf{Q}}_{k,21} & \hat{\mathbf{Q}}_{k,22} & \hat{\mathbf{Q}}_{k,32}^H \\ \hat{\mathbf{Q}}_{k,31} & \hat{\mathbf{Q}}_{k,32} & \hat{\mathbf{Q}}_{k,33} \end{bmatrix}, \quad \hat{\mathbf{\Xi}}_k = \begin{bmatrix} \hat{\mathbf{\Xi}}_{k,11} & \hat{\mathbf{\Xi}}_{k,21}^H & \hat{\mathbf{\Xi}}_{k,31}^H \\ \hat{\mathbf{\Xi}}_{k,21} & \hat{\mathbf{\Xi}}_{k,22} & \hat{\mathbf{\Xi}}_{k,32}^H \\ \hat{\mathbf{\Xi}}_{k,31} & \hat{\mathbf{\Xi}}_{k,32} & \hat{\mathbf{\Xi}}_{k,33} \end{bmatrix}, \quad (63)$$

where $\hat{\mathbf{Q}}_{k,11} \in \mathbb{C}^{N \times N}$, $\hat{\mathbf{Q}}_{k,21} \in \mathbb{C}^{N \times N}$, $\hat{\mathbf{Q}}_{k,22} \in \mathbb{C}^{N \times N}$, $\hat{\mathbf{Q}}_{k,31} \in \mathbb{C}^{M \times N}$, $\hat{\mathbf{Q}}_{k,32} \in \mathbb{C}^{M \times N}$, $\hat{\mathbf{Q}}_{k,33} \in \mathbb{C}^{M \times M}$ and $\hat{\mathbf{\Xi}}_{k,11} \in \mathbb{C}^{N \times N}$, $\hat{\mathbf{\Xi}}_{k,21} \in \mathbb{C}^{M \times N}$, $\hat{\mathbf{\Xi}}_{k,22} \in \mathbb{C}^{M \times M}$, $\hat{\mathbf{\Xi}}_{k,31} \in \mathbb{C}^{M \times N}$, $\hat{\mathbf{\Xi}}_{k,32} \in \mathbb{C}^{M \times M}$, $\hat{\mathbf{\Xi}}_{k,33} \in \mathbb{C}^{M \times M}$ denote sub-matrices of $\hat{\mathbf{Q}}_k$ and $\hat{\mathbf{\Xi}}_k$, respectively. Then, the Lagrangian function of (47) is given by

$$\begin{aligned} \bar{\mathcal{L}} = \sum_{k \in \mathcal{K}} & \left[\frac{\sum_{k \in \mathcal{K}} \text{Tr}(\mathbf{W}_k) T_{\text{Data}}}{T_{\text{MA}} + T_{\text{Data}}} - \text{Tr}(\mathbf{Z}_k \mathbf{W}_k) + \text{Tr}(\mathbf{A}_k \tilde{\mathbf{G}}_k^H \tilde{\mathbf{X}}_k \tilde{\mathbf{G}}_k) - \text{Tr}(\hat{\mathbf{Q}}_{k,22} \hat{\mathbf{T}}_k) - \text{Tr}(\hat{\mathbf{\Xi}}_{k,22} \mathbf{V}_k) \right] \\ & - 2\text{Re} \left\{ \sum_{k \in \mathcal{K}} \left[\text{Tr}(\hat{\mathbf{\Xi}}_{k,32} \mathbf{W}_k) + \text{Tr}((\hat{\mathbf{Q}}_{k,32} + \hat{\mathbf{\Xi}}_{k,21}) \mathbf{Y}_k) + \text{Tr}(\hat{\mathbf{Q}}_{k,21} \hat{\mathbf{X}}_k) \right] \right\} + \nu, \end{aligned} \quad (64)$$

where \mathbf{Z}_k and \mathbf{A}_k are the Lagrangian multiplier matrices associated with constraints $\mathbf{W}_k \geq \mathbf{0}$ and $\widehat{\text{C1}}$, respectively. Here, ν represents the collection of terms that do not involve optimization variables $\mathbf{W}_k, \mathbf{Y}_k, \hat{\mathbf{X}}_k, \hat{\mathbf{T}}_k$, and \mathbf{V}_k . For ease of representation, we denote the optimal variables for (47) with superscript "opt". The Karush–Kuhn–Tucker (KKT) conditions for (47) ignoring rank-one constraint C7 and binary constraint C3b are given by

$$\text{K1} : \mathbf{Z}_k^{\text{opt}} \geq \mathbf{0}, \mathbf{A}_k^{\text{opt}} \geq \mathbf{0},$$

$$\text{K2.1} : \mathbf{Z}_k^{\text{opt}} \mathbf{W}_k^{\text{opt}} = \mathbf{0},$$

$$\begin{aligned}
\text{K2.2 : } \mathbf{A}_k^{\text{opt}} \left(\mathbf{P}_k - \mathbf{G}_k^H \tilde{\mathbf{X}}_k \mathbf{G}_k \right) &= \mathbf{0}, \\
\text{K2.3 : } \hat{\mathbf{Q}}_{k,21}^{\text{opt}} \mathbf{B}^{\text{opt}} + \hat{\mathbf{Q}}_{k,22}^{\text{opt}} \mathbf{Y}_k^{\text{opt}} + (\hat{\mathbf{Q}}_{k,32}^{\text{opt}})^H &= \mathbf{0}, \\
\text{K2.4 : } \hat{\mathbf{\Xi}}_{k,21}^{\text{opt}} \mathbf{B}^{\text{opt}} + \hat{\mathbf{\Xi}}_{k,22}^{\text{opt}} \mathbf{W}_k^{\text{opt}} + (\hat{\mathbf{\Xi}}_{k,32}^{\text{opt}})^H &= \mathbf{0}, \\
\text{K3.1 : } \nabla_{\mathbf{W}_k} \bar{\mathcal{L}} = \mathbf{I}_M - \mathbf{Z}_k^{\text{opt}} - (\hat{\mathbf{\Xi}}_{k,32}^{\text{opt}} + (\hat{\mathbf{\Xi}}_{k,32}^{\text{opt}})^H) &= \mathbf{0}, \\
\text{K3.2 : } \nabla_{\mathbf{Y}_k} \bar{\mathcal{L}} = \hat{\mathbf{Q}}_{k,32}^{\text{opt}} + \hat{\mathbf{\Xi}}_{k,21}^{\text{opt}} &= \mathbf{0}, \\
\text{K3.3 : } \nabla_{\hat{\mathbf{T}}_k} \bar{\mathcal{L}} = \hat{\mathbf{Q}}_{k,22}^{\text{opt}} = \mathbf{0}, \nabla_{\mathbf{V}_k} \bar{\mathcal{L}} = \hat{\mathbf{\Xi}}_{k,22}^{\text{opt}} &= \mathbf{0}, \\
\text{K3.4 : } \nabla_{\hat{\mathbf{X}}_k} \bar{\mathcal{L}} = \sum_{k' \in \mathcal{K} \setminus k} \gamma_{k'} \tilde{\mathbf{G}}_{k'} \mathbf{A}_{k'}^{\text{opt}} \tilde{\mathbf{G}}_{k'}^H - \tilde{\mathbf{G}}_k \mathbf{A}_k^{\text{opt}} \tilde{\mathbf{G}}_k^H - (\mathbf{Q}_{k,21}^{\text{opt}} + (\mathbf{Q}_{k,21}^{\text{opt}})^H) &= \mathbf{0}, \quad \forall k \in \mathcal{K}.
\end{aligned} \tag{65}$$

From K3.3, we obtain $\hat{\mathbf{Q}}_{k,22}^{\text{opt}} = \mathbf{0}$ and $\hat{\mathbf{\Xi}}_{k,22}^{\text{opt}} = \mathbf{0}$. By substituting $\hat{\mathbf{Q}}_{k,22}^{\text{opt}} = \mathbf{0}$ and $\hat{\mathbf{\Xi}}_{k,22}^{\text{opt}} = \mathbf{0}$ into K2.3 and K2.4, respectively, we can rewrite K2.3 and K2.4 as follows

$$\begin{aligned}
\text{K2.3 : } (\hat{\mathbf{Q}}_{k,32}^{\text{opt}})^H &= -\hat{\mathbf{Q}}_{k,21}^{\text{opt}} \mathbf{B}^{\text{opt}}, \\
\text{K2.4 : } (\hat{\mathbf{\Xi}}_{k,32}^{\text{opt}})^H &= -\hat{\mathbf{\Xi}}_{k,21}^{\text{opt}} \mathbf{B}^{\text{opt}}.
\end{aligned} \tag{66}$$

Then, we substitute (66) into K3.2 and obtain

$$\hat{\mathbf{\Xi}}_{k,32}^{\text{opt}} + \mathbf{B}^{\text{opt}} \hat{\mathbf{Q}}_{k,21}^{\text{opt}} (\mathbf{B}^{\text{opt}})^H = \mathbf{0}. \tag{67}$$

Using the above result, we can rewrite K3.4 as follows

$$\hat{\mathbf{\Xi}}_{k,32}^{\text{opt}} + (\hat{\mathbf{\Xi}}_{k,32}^{\text{opt}})^H = 2\mathbf{B}^{\text{opt}} \left(\tilde{\mathbf{G}}_k \mathbf{A}_k^{\text{opt}} \tilde{\mathbf{G}}_k^H - \sum_{k' \in \mathcal{K} \setminus k} \gamma_{k'} \tilde{\mathbf{G}}_{k'} \mathbf{A}_{k'}^{\text{opt}} \tilde{\mathbf{G}}_{k'}^H \right) (\mathbf{B}^{\text{opt}})^H. \tag{68}$$

Hence, K3.1 can be recast as follows

$$\mathbf{Z}_k^{\text{opt}} = \mathbf{I}_M - 2\mathbf{B}^{\text{opt}} \left(\tilde{\mathbf{G}}_k \mathbf{A}_k^{\text{opt}} \tilde{\mathbf{G}}_k^H - \sum_{k' \in \mathcal{K} \setminus k} \gamma_{k'} \tilde{\mathbf{G}}_{k'} \mathbf{A}_{k'}^{\text{opt}} \tilde{\mathbf{G}}_{k'}^H \right) (\mathbf{B}^{\text{opt}})^H. \tag{69}$$

Then, we post-multiply (69) by $\mathbf{W}_k^{\text{opt}}$, i.e.,

$$2\mathbf{B}^{\text{opt}} \tilde{\mathbf{G}}_k \mathbf{A}_k^{\text{opt}} \tilde{\mathbf{G}}_k^H (\mathbf{B}^{\text{opt}})^H \mathbf{W}_k^{\text{opt}} = \left(\mathbf{I}_M + 2\mathbf{B}^{\text{opt}} \sum_{k' \in \mathcal{K} \setminus k} \gamma_{k'} \tilde{\mathbf{G}}_{k'} \mathbf{A}_{k'}^{\text{opt}} \tilde{\mathbf{G}}_{k'}^H (\mathbf{B}^{\text{opt}})^H \right) \mathbf{W}_k^{\text{opt}}. \tag{70}$$

Since $\mathbf{I}_M + 2\mathbf{B}^{\text{opt}} \sum_{k' \in \mathcal{K} \setminus k} \gamma_{k'} \tilde{\mathbf{G}}_{k'} \mathbf{A}_{k'}^{\text{opt}} \tilde{\mathbf{G}}_{k'}^H (\mathbf{B}^{\text{opt}})^H$ is full-rank, we obtain the following rank inequality

$$\begin{aligned}
\text{rank}(\mathbf{W}_k^{\text{opt}}) &= \text{rank} \left(\left(\mathbf{I}_M + 2\mathbf{B}^{\text{opt}} \sum_{k' \in \mathcal{K} \setminus k} \gamma_{k'} \tilde{\mathbf{G}}_{k'} \mathbf{A}_{k'}^{\text{opt}} \tilde{\mathbf{G}}_{k'}^H (\mathbf{B}^{\text{opt}})^H \right) \mathbf{W}_k^{\text{opt}} \right) \\
&= \text{rank} \left(\mathbf{B}^{\text{opt}} \tilde{\mathbf{G}}_k \mathbf{A}_k^{\text{opt}} \tilde{\mathbf{G}}_k^H (\mathbf{B}^{\text{opt}})^H \mathbf{W}_k^{\text{opt}} \right) \\
&\stackrel{(a)}{=} \text{rank} \left(\mathbf{B}^{\text{opt}} \mathbf{G}_k [\mathbf{I}_{L_k}, \bar{\boldsymbol{\psi}}_k] \mathbf{A}_k^{\text{opt}} [\mathbf{I}_{L_k}, \bar{\boldsymbol{\psi}}_k]^H \mathbf{G}_k^H (\mathbf{B}^{\text{opt}})^H \mathbf{W}_k^{\text{opt}} \right) \\
&\leq \min \{ \text{rank}(\mathbf{W}_k^{\text{opt}}), \text{rank}([\mathbf{I}_{L_k}, \bar{\boldsymbol{\psi}}_k] \mathbf{A}_k^{\text{opt}} [\mathbf{I}_{L_k}, \bar{\boldsymbol{\psi}}_k]^H) \},
\end{aligned} \tag{71}$$

where equality (a) holds due to $\tilde{\mathbf{G}}_k = \mathbf{G}_k[\mathbf{I}_{L_k}, \bar{\boldsymbol{\psi}}_k]$. Thus, we can prove $\text{rank}(\mathbf{W}_k^{\text{opt}}) \leq 1$ by showing that $\text{rank}([\mathbf{I}_{L_k}, \bar{\boldsymbol{\psi}}_k] \mathbf{A}_k^{\text{opt}} [\mathbf{I}_{L_k}, \bar{\boldsymbol{\psi}}_k]^H) \leq 1$. First, we obtain the following equalities [34]

$$\begin{aligned} \tilde{\mathbf{G}}_k[\mathbf{I}_{L_k}, \mathbf{0}]^T &= [\mathbf{G}_k \quad \mathbf{G}_k \bar{\boldsymbol{\psi}}_k][\mathbf{I}_N, \mathbf{0}]^T = \mathbf{G}_k, \quad \tilde{\mathbf{G}}_k = \mathbf{G}_k[\mathbf{I}_{L_k}, \bar{\boldsymbol{\psi}}_k], \\ \mathbf{P}_k[\mathbf{I}_{L_k}, \mathbf{0}]^T &= \begin{bmatrix} q_k \mathbf{I}_{L_k} & \mathbf{0} \\ \mathbf{0} & -q_k \epsilon_k^2 - \sigma_k^2 \gamma_k \end{bmatrix} \begin{bmatrix} \mathbf{I}_{L_k} \\ \mathbf{0} \end{bmatrix} = \begin{bmatrix} q_k \mathbf{I}_{L_k} \\ \mathbf{0} \end{bmatrix} = q_k[\mathbf{I}_{L_k}, \bar{\boldsymbol{\psi}}_k]^H - [\mathbf{0}, q_k \bar{\boldsymbol{\psi}}_k]^H. \end{aligned} \quad (72)$$

Then, we pre-multiply $[\mathbf{I}_{L_k}, \bar{\boldsymbol{\psi}}_k]$ and post-multiply K2.2 by $[\mathbf{I}_{L_k}, \mathbf{0}]^T$, respectively, and rewrite the resulting equation as follows

$$\begin{aligned} [\mathbf{I}_{L_k}, \bar{\boldsymbol{\psi}}_k] \mathbf{A}_k^{\text{opt}} \left(q_k[\mathbf{I}_{L_k}, \bar{\boldsymbol{\psi}}_k]^H - [\mathbf{0}, q_k \bar{\boldsymbol{\psi}}_k]^H - [\mathbf{I}_{L_k}, \bar{\boldsymbol{\psi}}_k]^H \mathbf{G}_k^H \tilde{\mathbf{X}}_k \mathbf{G}_k \right) &= \mathbf{0}, \\ [\mathbf{I}_{L_k}, \bar{\boldsymbol{\psi}}_k] \mathbf{A}_k^{\text{opt}} [\mathbf{I}_{L_k}, \bar{\boldsymbol{\psi}}_k]^H (q_k \mathbf{I}_{L_k} - \mathbf{G}_k^H \tilde{\mathbf{X}}_k \mathbf{G}_k) &= [\mathbf{I}_{L_k}, \bar{\boldsymbol{\psi}}_k] \mathbf{A}_k^{\text{opt}} [\mathbf{0}, q_k \bar{\boldsymbol{\psi}}_k]^H. \end{aligned} \quad (73)$$

According to constraint $\widehat{\text{C1}}$, we have

$$\begin{bmatrix} q_k \mathbf{I}_{L_k} - \mathbf{G}_k^H \tilde{\mathbf{X}}_k \mathbf{G}_k & -\mathbf{G}_k^H \tilde{\mathbf{X}}_k \mathbf{G}_k \bar{\boldsymbol{\psi}}_k \\ -\bar{\boldsymbol{\psi}}_k^H \mathbf{G}_k^H \tilde{\mathbf{X}}_k \mathbf{G}_k & -q_k \epsilon_k^2 - \sigma_k^2 \gamma_k - \bar{\boldsymbol{\psi}}_k^H \mathbf{G}_k^H \tilde{\mathbf{X}}_k \mathbf{G}_k \bar{\boldsymbol{\psi}}_k \end{bmatrix} \geq \mathbf{0}. \quad (74)$$

Hence, we can claim that $q_k \mathbf{I}_{L_k} - \mathbf{G}_k^H \tilde{\mathbf{X}}_k \mathbf{G}_k \geq \mathbf{0}$ is non-singular [34]. Since multiplication by a non-singular matrix will not alter the rank of a matrix, the following rank property holds

$$\text{rank}([\mathbf{I}_{L_k}, \bar{\boldsymbol{\psi}}_k] \mathbf{A}_k^{\text{opt}} [\mathbf{I}_{L_k}, \bar{\boldsymbol{\psi}}_k]^H) = \text{rank}([\mathbf{I}_{L_k}, \bar{\boldsymbol{\psi}}_k] \mathbf{A}_k^{\text{opt}} [\mathbf{0}, q_k \bar{\boldsymbol{\psi}}_k]^H) \leq 1. \quad (75)$$

Thus, based on (71), we have

$$\text{rank}(\mathbf{W}_k^{\text{opt}}) \leq \text{rank}([\mathbf{I}_{L_k}, \bar{\boldsymbol{\psi}}_k] \mathbf{A}_k^{\text{opt}} [\mathbf{I}_{L_k}, \bar{\boldsymbol{\psi}}_k]^H) \leq 1. \quad (76)$$

This completes the proof of Theorem 1.

REFERENCES

- [1] Y. Wu *et al.*, "Movable antenna-enhanced multiuser communication: Jointly optimal discrete antenna positioning and beamforming," in *Proc. IEEE Global Commun. Conf. (GLOBECOM)*. Kuala Lumpur, Malaysia, Dec. 2023, pp. 1–6.
- [2] J. Mietzner *et al.*, "Multiple-antenna techniques for wireless communications - a comprehensive literature survey," *IEEE Commun. Surv. Tuts.*, vol. 11, no. 2, pp. 87–105, 2009.
- [3] S.-H. Tsai and H. V. Poor, "Power allocation for artificial-noise secure MIMO precoding systems," *IEEE Trans. Signal Process.*, vol. 62, no. 13, pp. 3479–3493, Jul. 2014.
- [4] D. Xu *et al.*, "Robust and secure resource allocation for ISAC systems: A novel optimization framework for variable-length snapshots," *IEEE Trans. Commun.*, vol. 70, no. 12, pp. 8196–8214, Dec. 2022.
- [5] C. Huang *et al.*, "Holographic MIMO surfaces for 6G wireless networks: Opportunities, challenges, and trends," *IEEE Wirel. Commun.*, vol. 27, no. 5, pp. 118–125, Oct. 2020.
- [6] D. Xu *et al.*, "Resource allocation for IRS-assisted full-duplex cognitive radio systems," *IEEE Trans. Commun.*, vol. 68, no. 12, pp. 7376–7394, Dec. 2020.
- [7] L. Zhu *et al.*, "Modeling and performance analysis for movable antenna enabled wireless communications," *IEEE Trans. Wireless Commun.*, vol. 23, no. 6, pp. 6234–6250, 2024.
- [8] W. Ma *et al.*, "MIMO capacity characterization for movable antenna systems," *IEEE Trans. Wireless Commun.*, vol. 23, no. 4, pp. 3392–3407, 2024.
- [9] K.-K. Wong *et al.*, "Fluid antenna systems," *IEEE Trans. Wireless Commun.*, vol. 20, no. 3, pp. 1950–1962, 2020.
- [10] L. Zhu *et al.*, "Movable-antenna enhanced multiuser communication via antenna position optimization," *IEEE Trans. Wireless Commun.*,

vol. 23, no. 7, pp. 7214–7229, 2024.

- [11] L. o. Zhu, “Movable antennas for wireless communication: Opportunities and challenges,” *IEEE Commun. Mag.*, vol. 62, no. 6, pp. 114–120, 2024.
- [12] K.-K. Wong and K.-F. Tong, “Fluid antenna multiple access,” *IEEE Trans. Wireless Commun.*, vol. 21, no. 7, pp. 4801–4815, 2021.
- [13] A. Zhuravlev *et al.*, “Experimental simulation of multi-static radar with a pair of separated movable antennas,” in *Proc. of IEEE Int. Conf. Microwaves, Commun. Antennas and Electron. Syst.*, Nov, 2015, pp. 1–5.
- [14] S. Basbug, “Design and synthesis of antenna array with movable elements along semicircular paths,” *IEEE Antennas Wirel. Propag. Lett.*, vol. 16, pp. 3059–3062, 2017.
- [15] W. Ma *et al.*, “Compressed sensing based channel estimation for movable antenna communications,” *IEEE Commun. Letters*, vol. 27, no. 10, pp. 2747–2751, 2023.
- [16] Z. Xiao *et al.*, “Channel estimation for movable antenna communication systems: A framework based on compressed sensing,” *IEEE Trans. Wireless Commun.*, 2024, early access, doi=10.1109/TWC.2024.3385110.
- [17] X. Chen *et al.*, “Joint beamforming and antenna movement design for moveable antenna systems based on statistical CSI,” in *Proc. IEEE Global Commun. Conf.* Kuala Lumpur, Malaysia, Dec. 2023, pp. 4387–4392.
- [18] Y. Ye *et al.*, “Fluid antenna-assisted MIMO transmission exploiting statistical CSI,” *IEEE Commun. Letters*, 2023.
- [19] N. D. Nguyen *et al.*, “Compact model for 3d printer energy estimation and practical energy-saving strategy,” *Electronics*, vol. 10, no. 4, p. 483, 2021.
- [20] D. Xu *et al.*, “Optimal resource allocation design for large IRS-assisted SWIPT systems: A scalable optimization framework,” *IEEE Trans. Commun.*, vol. 70, no. 2, pp. 1423–1441, 2022.
- [21] Y. Wu *et al.*, “Globally optimal resource allocation design for irs-assisted multiuser networks with discrete phase shifts,” in *2023 IEEE Int. Conf. Commun. Workshops (ICC Workshops)*, 2023, pp. 1216–1221.
- [22] S. Hu *et al.*, “Robust and secure sum-rate maximization for multiuser MISO downlink systems with self-sustainable IRS,” *IEEE Trans. Commun.*, vol. 69, no. 10, pp. 7032–7049, 2021.
- [23] Z.-Q. Luo and W. Yu, “An introduction to convex optimization for communications and signal processing,” *IEEE J. Sel. Areas Commun.*, vol. 24, no. 8, pp. 1426–1438, 2006.
- [24] R. Zhang *et al.*, “Joint beamforming and power control for multiantenna relay broadcast channel with QoS constraints,” *IEEE Trans. Signal Process.*, vol. 57, no. 2, pp. 726–737, Feb. 2008.
- [25] M. Grant and S. Boyd, “CVX: Matlab software for disciplined convex programming, version 2.1,” <http://cvxr.com/cvx>, Jan. 2020.
- [26] R. Horst and H. Tuy, *Global optimization: Deterministic approaches*. Springer Science & Business Media, 2013.
- [27] S. Boyd and J. Mattingley, “Branch and bound methods,” *Notes for EE364b, Stanford University*, vol. 2006, p. 07, 2007.
- [28] L. Thi *et al.*, “Exact penalty and error bounds in DC programming,” *Journal of Global Optimization*, vol. 52, no. 3, pp. 509–535, 2012.
- [29] D. W. K. Ng and R. Schober, “Secure and green SWIPT in distributed antenna networks with limited backhaul capacity,” *IEEE Trans. Wireless Commun.*, vol. 14, no. 9, pp. 5082–5097, 2015.
- [30] I. M. Bomze *et al.*, “Interior point methods for nonlinear optimization,” *Nonlinear Optimization: Lectures given at the CIME Summer School held in Cetraro, Italy, July 1-7, 2007*, pp. 215–276, 2010.
- [31] M. Razaviyayn *et al.*, “A unified convergence analysis of block successive minimization methods for nonsmooth optimization,” *SIAM Journal on Optimization*, vol. 23, no. 2, pp. 1126–1153, 2013.
- [32] S. P. Boyd and L. Vandenberghe, *Convex optimization*. Cambridge University Press, 2004.
- [33] X. Yu *et al.*, “IRS-assisted green communication systems: Provable convergence and robust optimization,” *IEEE Trans. Commun.*, vol. 69, no. 9, pp. 6313–6329, Sept. 2021.
- [34] F. Alavi *et al.*, “Robust beamforming techniques for non-orthogonal multiple access systems with bounded channel uncertainties,” *IEEE Commun. Lett.*, vol. 21, no. 9, pp. 2033–2036, 2017.

- [35] Y. Wu *et al.*, “Globally optimal resource allocation design for discrete phase shift IRS-assisted multiuser networks with perfect and imperfect CSI,” *arXiv preprint arXiv:2310.04063*, 2023.
- [36] Faulhaber, *Stepper Motors, Series AM2224*, 2023. [Online]. Available: https://www.faulhaber.com/fileadmin/Import/Media/EN_AM2224_FPS.pdf
- [37] G. McLean, “Review of recent progress in linear motors,” in *IEE Proceedings B (Electric Power Applications)*, vol. 135, no. 6. IET, 1988, pp. 380–416.
- [38] S. Sanayei and A. Nosratinia, “Antenna selection in MIMO systems,” *IEEE Commun. Mag.*, vol. 42, no. 10, pp. 68–73, Oct. 2004.
- [39] U. Rashid *et al.*, “Joint optimization of source precoding and relay beamforming in wireless MIMO relay networks,” *IEEE Trans. Commun.*, vol. 62, no. 2, pp. 488–499, Feb. 2014.